FFIBM/786/115

SINGLE SHOT INVERSION FROM THE L-ANTENNA EXPERIMENT IN 1999

EIDEM Ellen Johanne

FFI/RAPPORT-2001/02927

FORSVARETS FORSKNINGSINSTITUTT (FFI)
Norwegian Defence Research Establishment

UNCLASSIFIED

P O BOX 25
N0-2027 KJELLER, NORWAY
REPORT DOCUMENTATION PAGE

SECURITY CLASSIFICATION OF THIS PAGE
(when data entered)

1) PUBL/REPORT NUMBER	2) SECURITY CLASSIFICATION	3) NUMBER OF
FFI/RAPPORT-2001/02927	UNCLASSIFIED	PAGES
1a) PROJECT REFERENCE	2a) DECLASSIFICATION/DOWNGRADING SCHEDULE	63
FFIBM/786/115	-	

4) TITLE

SINGLE SHOT INVERSION FROM THE L-ANTENNA EXPERIMENT IN 1999

5) NAMES OF AUTHOR(S) IN FULL (surname first)

EIDEM Ellen Johanne

6) DISTRIBUTION STATEMENT

Approved for public release. Distribution unlimited. (Offentlig tilgjengelig)

7) INDEXING TERMS

IN ENGLISH:	IN NORWEGIAN:
a) Matched field processing	a) Mediatilpasset signalbehandling
b) Localization	b) Lokalisering
c) Geoacoustic properties	c) Geoakustiske egenskaper
d) Broadband	d) Bredbånd
e) Shallow water	e) Grunt vann

THESAURUS REFERENCE:

8) ABSTRACT

Matched field processing techniques have been tested out in this report on a single shot from the 1999 L-antenna experiment. Inversions for geoacoustic and geometric parameters were carried out at five frequencies between 22.9 Hz and 87.6 Hz with different results. The baseline model consisted of three water layers and a sediment layer overlying the half-space substrate. The environment was assumed range-independent with no shear waves. Mainly, it was inverted for water depth, sediment thickness, sediment velocity and substrate velocity. The best results were obtained at 48.9 Hz. Source localization was carried out at different frequencies with the baseline model and with the baseline model incorporating three GA estimated parameters inverted at 48.9 Hz. The OASES module OAST and SAGA with genetic algorithms were used for forward modelling and inversion. In addition, the time responses were simulated using the OASES module OASP.

9) DATE	AUTHORIZED BY This page only	POSITION
5 November 2001	Jarl Johnsen	Director of Research

UNCLASSIFIED

ISBN 82-464-0555-1

SECURITY CLASSIFICATION OF THIS PAGE
(when data entered)

CONTENTS

SINGLE SHOT INVERSION FROM THE L-ANTENNA EXPERIMENT IN 1999

1 INTRODUCTION

A matched field processing experiment using a 1040 m hydrophone array was conducted in the Barents Sea from 2 – 8 August 1999 (1)(2). The measurement area was at Nordkappbanken, outside the Tana fiord. The source vessel sailed one broad side run away from the antenna and two end-fire runs towards the antenna. In total 355 explosive charges were deployed during these three runs. Detonation times and source signals were recorded onboard the source vessel K/V Polarvakt using a single, towed hydrophone. The array was deployed in an upright L-shape at approximately 319 m depth. The receiver station was onboard R/V H U Sverdrup II, which also deployed and retrieved the antenna. A few days after the acoustic experiment (in the period 10 – 12 August 1999) seismic reflection and refraction measurements were carried out from R/V H U Sverdrup II along the three run lines (3). Detailed experimental description is given in Chapter 2. Originally, a shot detonated at a depth of 91 m or 244 m was preferred for matched field processing in order to avoid noise due to bubbles in the surface, but for these depths the pulse arrivals were not as clear as for the 18 m shots. It was desired to analyse a shot 3 – 5 km from the antenna, at sufficient distance to be out of the near field, but close enough to assume range independence. Closest to the antenna the smaller MK 64 charges were dropped. However, the source spectrum of these charges is not as well known as the source spectrum of MK61 and MK82. Minimum array tilt was also a requirement. With these requirements shot 112 in run 1 with nominal detonation depth 18 m, at range about 6 km and with 0.82 kg TNT was selected for further analyses.

Based on the experimental data and results from the seismic measurements, a first-order geoacoustic model (also called the baseline model) is presented in Chapter 3. In order to understand the measured time responses the OASES module OASP (4) is used to simulate time responses on the receiver antenna for the first-order geoacoustic model and modifications of this. Comparison of measured and simulated time responses are presented and discussed in Chapter 4.

In Chapter 5 matched field inversions for geometric and geoacoustic properties are carried out using SAGA (Seismo Acoustic inversion using Genetic Algorithms) (5) and the OASES module OAST. The environment is assumed range independent and no shear effects are addressed. As input to SAGA the covariance matrix is computed for the measured data at selected frequencies. At first, single frequency inversion was intended, with a frequency between 10 – 20 Hz. Due to noise in the acoustic data, higher frequencies were preferred. OAST is used to compute the simulated complex pressure vector at similar frequencies. The Bartlett processor is used as the objective function, and the optimisation is carried out to find the optimum model parameter vector that minimizes the selected objective function. For minimising the objective function, genetic algorithms are used.

Efforts have been put in to understand different aspects of SAGA using the Bartlett objective function with the covariance matrix as input. This has been time consuming, since the manual (5) is not as detailed as it could have been. Algorithms, normalization factors and plotting results are outlined in Chapter 5 and in appendix.

Source localization (matched field procedures for localization) is carried out at different frequencies in Chapter 6. SAGA and the OASES module OAST are used in a similar way as with the geoacoustic inversions. The parameter search space for source depth is 1 – 315 m, covering about the whole water column. The parameter search space for range is 1 – 20 km.

This report is the first on matched field inversion and localization on the data from the L-antenna experiment in 1999. Some of the aspects in matched field processing are addressed in the report in context with the selected shot. Other aspects need to be revealed in following reports. A summary of the report and recommendations for future work is outlined in Chapter 7.

2   EXPERIMENTAL CONFIGURATION

2.1   Shot selected for analyses

Shot 112 in run 1 was launched from the source vessel K/V Polarvakt at 02:24 on 5 August 1999. The launching angle was 20° from starboard side. The nominal detonation depth was 18 m and the type of charge was MK61 (0.82 kg TNT). The source vessel recorded GPS position at each shot and the range from the detonation position of shot 112 to the planned array position was 6.4 km, see Appendix A. The range distance from the detonation position of shot 112 to the vertical antenna was estimated to be 5910 m (6). The uncertainty is easily ± 20 m and in order of magnitude equal to the wavelengths selected for inversions.

2.2   Array configuration and tilt

The antenna was deployed in an upright L-shape (refer Chapter 2.4.1). The vertical part consisted of 21 hydrophones with spacing 10 m. The horizontal part of the array consisted of 10 hydrophones with spacing from 20 m – 240 m as shown in Figure 2.1. The hydrophones had either 12 dB or 32 dB gain. The sampling frequency was 3051.8 Hz, and the data were recorded in sequences of 506 samples with time tagging (GPS time). Detailed descriptions of the array configuration and acquisition system are found in (7) and (8).

The tilt of the vertical antenna was monitored continuously during the experiment using three Aquadopp current meters. The current meters were fastened to the array cable with strips and tapes approximately 194 m, 104 m and 14 m above the lowest hydrophone. The tilts of the lowest, middle and upper current meter were at most 14°, 10° and 6°, respectively. At the end of run 1 the tilts were at minimum (4 - 5°, 0.2° and 0.2°). Two possible situations of the cable curvature are modelled in Appendix A. In both cases and with an acoustic source signal of 50 – 100 Hz the horizontal displacements were well below the wavelength of the signal (30 –

15 m). The uncertainties in range and the depth variation over the 5.9 km are more dramatically.
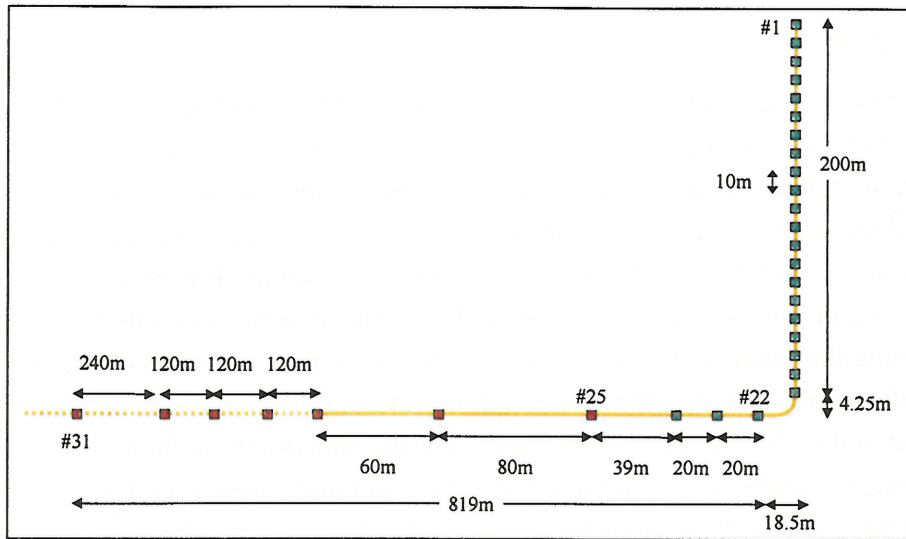

Figure 2.1   *The array configuration in August 1999. The vertical part was ESE of the planned array position. The bearing of the horizontal part was 295.7°. The green hydrophones had 12 dB gain, while the red hydrophones had 32 dB gain.*

2.3   Oceanography

During the acoustic experiment CTD measurements were taken at the receiver position and the sound speed profiles are plotted in Appendix B. In general there was a warmer surface layer of thickness 20 – 40 m, with sound velocity 1481 – 1488 m/s, and a colder bottom layer with sound velocity down to 1463 m/s. Thus the profiles were downward refracting. The average sound velocity during the experiment was 1472 m/s at the receiver position. At the source position XCTD's, XSV's and XBT's were dropped. The sound speed profiles computed from the XCTD's are plotted in Appendix B. In general, the tendency is the same at both the source position and receiver position. The sound speed profile was measured using an XCTD at the source position at 02:35 on 5 August, only a few minutes after the launching of the shot selected for analysis in this report. The measured data shows that the average sound speed in the water column at this moment was 1473 m/s.

2.4   Bathymetry

2.4.1   Hydrophone depths and water depth at receiver position

The average water depth at the antenna position was measured indirectly from the pressure sensors within the upper two Aquadopp current meters. The two pressure sensors recorded their depths continuously during the experiment, while a pressure sensor within the third current meter was too deep to operate. During the deployment of the antenna, the water depth was measured using an EA 500 echo sounder from Simrad (38 kHz). Analyses of the data from both of these measurements indicate that the water depth at the antenna position (vertical part) was 319 m ± 1 m, see Appendix C. Assuming a water depth of 319 m, the depth of the lowest

hydrophone was 315 m, while the depth of the upper hydrophone was 115 m at minimum tilt (and minimum current velocity).

2.4.2   Topography

During the acoustic experiment the source vessel recorded time and GPS position for each shot, but the bathymetry data from the echo sounder onboard the source vessel was not logged. However, seismic reflection and refraction measurements were carried out a few days later as mentioned and the seismic vessel sailed the same three run lines (3). During the last part of run 1 the seismic vessel followed the track of the source vessel quite well as shown in Figure 2.2. The water depth was continuously measured from the seismic vessel using the same echo sounder as during the deployment of the antenna. Since the tidal variations were not measured, the water depths recorded during the seismic survey are manually adjusted to have a water depth of 319 m at the vertical antenna. In Figure 2.3 the bathymetry at the last part of run 1 (near the antenna) is shown. As seen the water depth decreases slowly as the vessel is approaching the array. Over a distance of 10 km, the reduction is 40 m. The spikes are probably due to interference with the parabolic sonar onboard the vessel. The water depth at the detonation position of the shot selected for analysis in this report (5.9 km east off the receiver position) was 332 - 333 m. Thus the average water depth between the source and receiver position was approximately 326 m. The depth change was about 14 m.
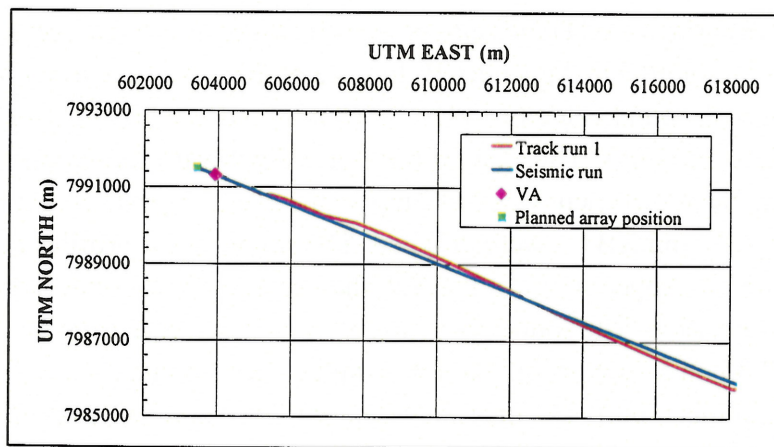

Figure 2.2   *The track of the source vessel during the last part of run1 and the corresponding track of he seismic vessel during the seismic run a few days later. The position of the array's vertical part and the planned array position are marked.*
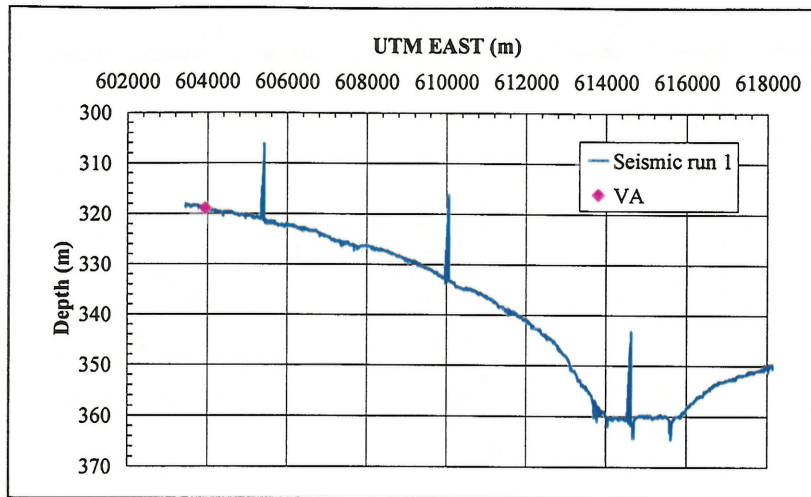
Figure 2.3   *The bottom profile for the last 14 km of run 1. The spikes are probably due to interference with the parabolic sonar (TOPAS) onboard the survey vessel. The water depth at the source position, 5.9 km east of the receiver position, was 332 – 333 m. The depth change was about 14 m.*

3   GEOACOUSTIC MODEL

3.1   Seismic reflection and refraction measurements

Seismic reflection and refraction measurements were as mentioned carried out from 10 – 12 August 1999. The three seismic run lines and 15 WABR measurements sites are shown in Figure 3.1. The estimated sound velocities for the upper bedrock are listed in Table 3.1. Except for three sites the sound velocity varied between 2210 m/s – 2420 m/s.

Analysing the acoustic data received at the antenna, refracted pulses are easy to observe on the horizontal antenna (H25-H31), especially for the shallow charges (nominal detonation depth 18 m). On the vertical antenna the refracted pulses are not easy to observe due to low-frequent noise. Analysis of several shots in run 1 shows that the travel time of the refracted pulses over the horizontal hydrophones (spanning 740 m) increased with range. Computing the sound velocity from the inverse of the slope for both the direct pulses and the refracted pulses, an increasing bedrock velocity versus range was found, while the water sound velocity is in average 1486 ± 6 m/s, approximately as expected, see Figure 3.2. The increase in sound velocity with distance for the refracted waves may indicate a gradient sound velocity in the bedrock. It is not possible to observe the wave refracted at the water-sediment interface, due to continuously refracted waves from the bedrock.

The true arrival times of the direct and refracted waves at hydrophone 25 are plotted in Figure 3.3. At range 5.9 km the refracted waves arrive the antenna about 2 s earlier than the direct waves. Straight lines are drawn between the measurement sites. These lines more or less follow a curve, as will be the case if the bedrock has continuous velocity change with depth. A trend line is plotted for each line and the slope and intersection with the time axis is computed. From these data and assumptions of the sediment layer, it is possible to estimate the bedrock sound velocity and thickness of the refracting "layer" or turning point.
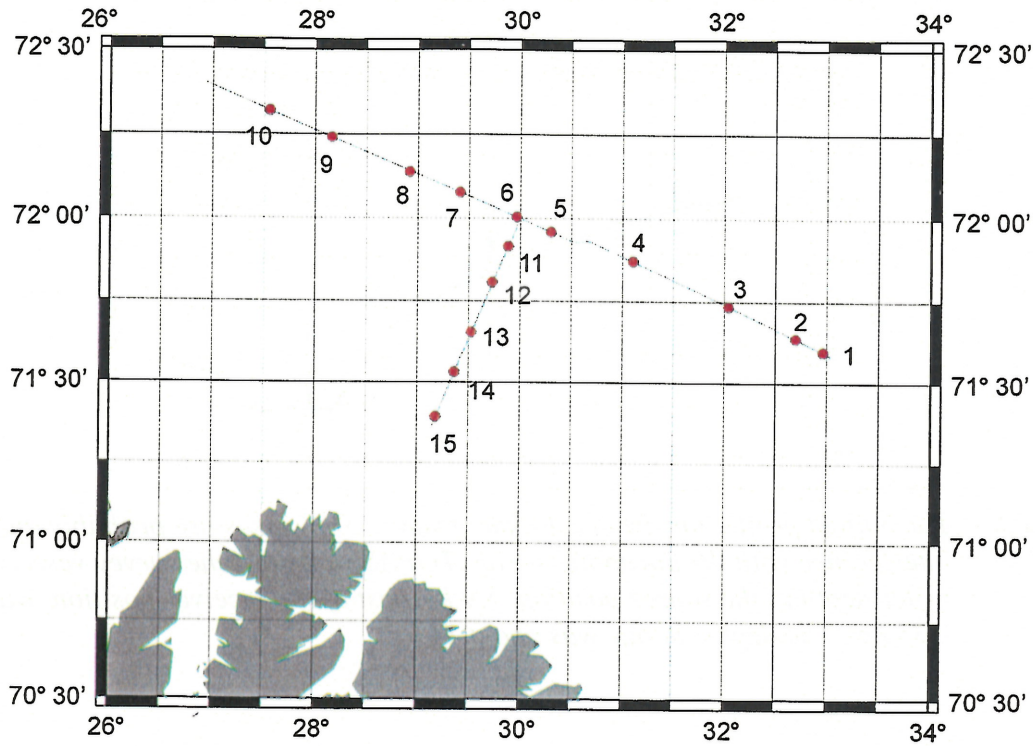
Figure 3.1   *The WABR measurements and seismic run lines in August 1999.*

WABR #	Latitude (deg)	Longitude (deg)	Sound velocity upper bedrock (m/s)
1	71.5963	32.9655	2210
2	71.6372	32.6987	2310
3	71.7358	32.0437	2230
4	71.8718	31.1043	2350
5	71.9588	30.3022	2370
6	72.0045	29.9658	2420
7	72.0772	29.4122	2370
8	72.1380	28.9208	2200
9	72.2407	28.1623	2590
10	72.3193	27.5560	3840
11	71.9157	29.8828	2210
12	71.8070	29.7297	2420
13	71.6538	29.5245	2220
14	71.5312	29.3613	2410
15	71.3933	29.1803	1850/2430

Table 3.1   *Estimations of the sound velocity in the upper bedrock based on 15 WABR measurements in August 1999.*
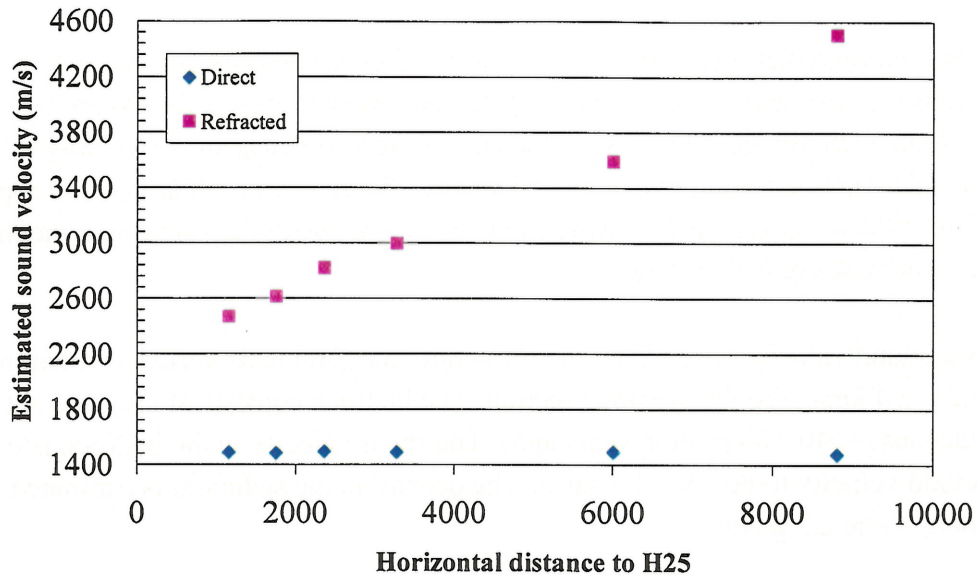
Figure 3.2   *The inverse of the slope over the horizontal hydrophones (H25 – H31) shows an increasing bedrock sound velocity as the distance between the source and receiver increases. The increase with range may indicate a gradient sound velocity in the bedrock.*
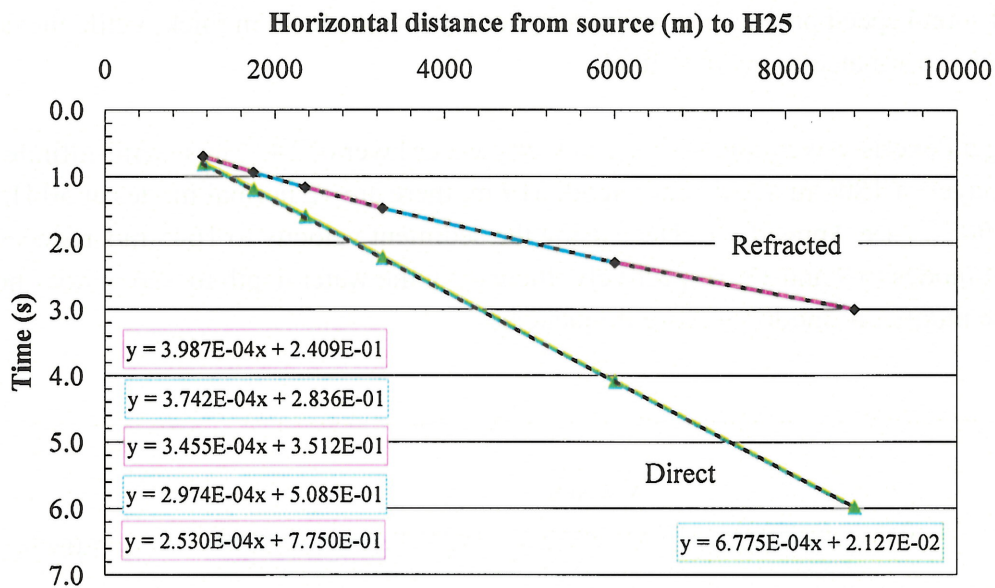
Figure 3.3   *Observed time of arrival of direct pulses and refracted pulses for different shots in run 1. Straight lines are drawn between the different measurement sites, and trend lines are computed for each section.*

3.2   First-order geoacoustic model

Analyses of the seismic reflection and refraction measurements indicate a two-layer bottom, with a sediment layer above the semi-infinite bedrock (3). The sediment layer is assumed having constant sound velocity and density, and no shear velocity. The sediment sound velocity is found from the literature to be 1770 m/s (3). The density in the sediment is estimated from the sound velocity to be 2.0 g/cm^3 (3).

The reflection measurements give the two-way travel time of the sediment layer. For run 1 the sediment thickness varied from less than 9 m (the resolution of the system) to 39 m, assuming a sediment sound velocity of 1800 m/s. At the end of run 1, the measured two-way travel time was 41 ms and assuming a sound velocity of 1800 m/s the sediment thickness was approximately 37 m. If the average sound velocity in the layer was lower than assumed, the thickness of the layer would be equivalent lower.

The bedrock sound velocity found from the refraction measurements varied as mentioned between 2.2 – 2.4 km/s, see the previous section. The bedrock consists of clay and silt from the Early Cretaceous (~140-100 million years ago). The shear velocity in the bedrock is estimated from the sound velocity to be 0.9 – 1.1 km/s. The density in the sediment is estimated from the sound velocity to be 2.2 g/cm^3.

Figure 3.4 shows the first-order geoacoustic (baseline) model for run 1, based on the results from the analysis of the seismic measurements. For simplicity there is assumed range-independence and no shear effects. Because of the low resolution, there could be an upper sediment layer of a few metres not observable in the seismic data.

In the baseline model the water column is divided into three layers in coherence with the measured sound speed profile. The warmer upper layer is made 30 m thick, while the colder lower layer is estimated to be 44 m thick.

Assuming a Pekeris waveguide with iso-velocity water layer of 1473 m/s, semi-infinite sediment layer of 1800 m/s and water depth 319 m, there are 12 normal modes at 50 Hz and 22 modes at 90 Hz, see Appendix E. Decreasing the sediment velocity to 1645 m/s reduces the number of modes to 9 and 17, respectively. Increasing the water depth to 326 m does not change the number of modes at these frequencies.
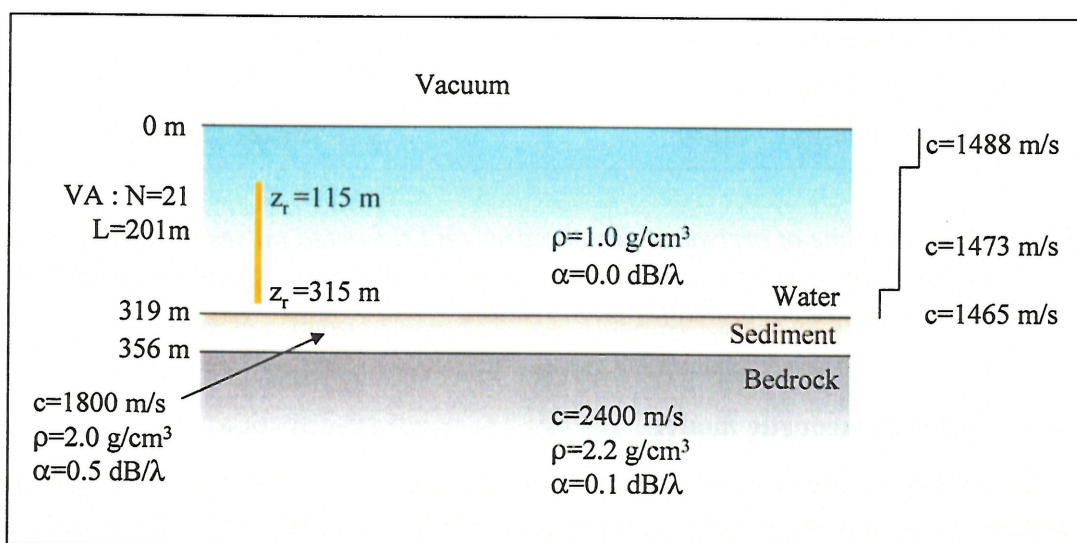

Figure 3.4   First-order geo-acoustic model for the shot selected for analysis in this report.

4   MEASURED AND SIMULATED TIME RESPONSES

Figure 4.1 shows the pulse arrivals of shot 112 during 400 ms. Low-frequent noise is dominating at frequencies below 20 –30 Hz and bandpass filtering the data, is easy to identify several bottom and surface reflections of the pulses. The time of detonation recorded by the single hydrophone towed behind the source vessel was 02:24:07.510005 Z on 5/8-99. Taking into account the travel time between the detonation position and the towed hydrophone, which was estimated to be 23 ms (6), the actual time of detonation was 02:24:07.487 Z. The observed data indicates that the shock pulse arrived the upper hydrophone at 02:24:11.526 Z. The time delay between the detonation and presumable first arrival at the antenna was hence 4039 ms. However, assuming a constant water sound velocity of 1473 m/s, the estimated time delay between the detonation and arrival at the upper hydrophone is 4013 ms, which makes a difference of 26 ms. Zooming in at the beginning of the shot, it is possible to observe very weak bottom-reflected pulses. The higher up in the water column, the stronger these bottom-reflected pulses are. Ray-tracing shows that a downward refracting sound velocity profile like measured prohibits the arrival of the direct pulses at ranges above approximately 5 km. At range 5.9 km the bottom-reflected pulses are only possible to see at the shallowest hydrophones. Hence, the presumable direct pulses are in fact the bottom-surface-reflected pulses. The surface-reflected pulses are 0.5 - 1.2 ms delayed compared to the direct pulses, hence interfering with the direct pulse and not easily identified.

4.1   Bubble pulses and reflections

The first bubble pulse period of each of the detonated charges was estimated from the acoustic signals received at the single hydrophone towed behind the source vessel. The first bubble pulse period of the shot selected for analysis in this report was 125.55 ms, indicating a detonation depth of 17.2 m according to Equation (D.5) in Appendix D. This bubble pulse period is confirmed by the acoustic data received at the antenna. According to the theory in Appendix D, the second bubble pulse is expected 214 ms after the shock pulse. However, the measured time delay between the shock pulse and the second bubble pulse was approximately 227 ms. The difference of 13 ms between theory and measurement is probably due to the vertical migration effect or buoyancy of the bubble, which cannot be ignored for 0.82 kg charges detonating at depths shallower than 60 m (9) (10). A period of 227 ms indicates an actual depth of 15.3 m. It is not possible to observe the third bubble pulse in the acoustic data received at the antenna. Table 4.1 summarizes these results.

For a 0.82 kg charge detonating at a depth of 17.2 m at a range of 5.91 km from the receiver, the peak pressure of the shock pulse is $P_0 = 2.56 \cdot 10^9 \mu Pa$, according to Equation (D.7). The pressures of the first and second bubble pulses relative to the shock pulse pressure are $P_1/P_0 = 0.27$ and $P_2/P_0 = 0.06$, respectively. The measured data indicate however larger relative pressures, especially for the second bubble pulse. This may be due to surface reflection interference.

The spectra of 40 sequences of the vertical hydrophones are shown in Figure 4.2. There are several peaks below 10 Hz, which are mainly due to noise. Computing the spectra of nearby charges, it is seen that the frequency of the three first peaks does not change with the charge depth. Below 10 Hz the spectrum levels of the horizontal hydrophones are considerable lower than the spectrum levels of the vertical hydrophones, indicating that the motion of the vertical antenna is causing the noise. However, with a detonation depth of 17.2 m, the peak at approximately 8.0 Hz fits with the fundamental bubble frequency.

	Bubble pulse number		
	1	2	3
Measured bubble period T$_i$ (arrival time after shock pulse)	125.6 ms	101 ms (227 ms)	Not observed
Calculated bubble period T$_i$ (arrival time after shock pulse)		88.1 ms (213.6 ms)	71.4 ms (285.0 ms)

Table 4.1   The bubble pulse periods for a 0.82 kg TNT charge with detonation depth z = 17.2 m.
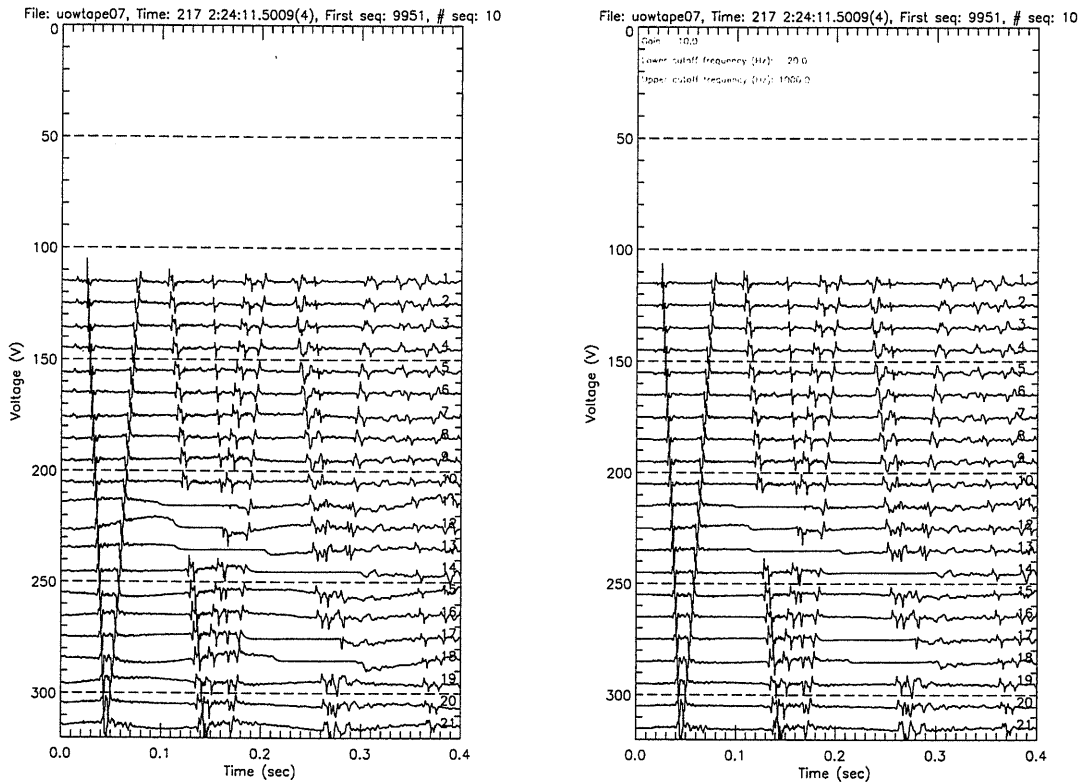

Figure 4.1   The pulse arrivals of shot 112 unfiltered (left) and band pass filter 20 − 1000 Hz (right).
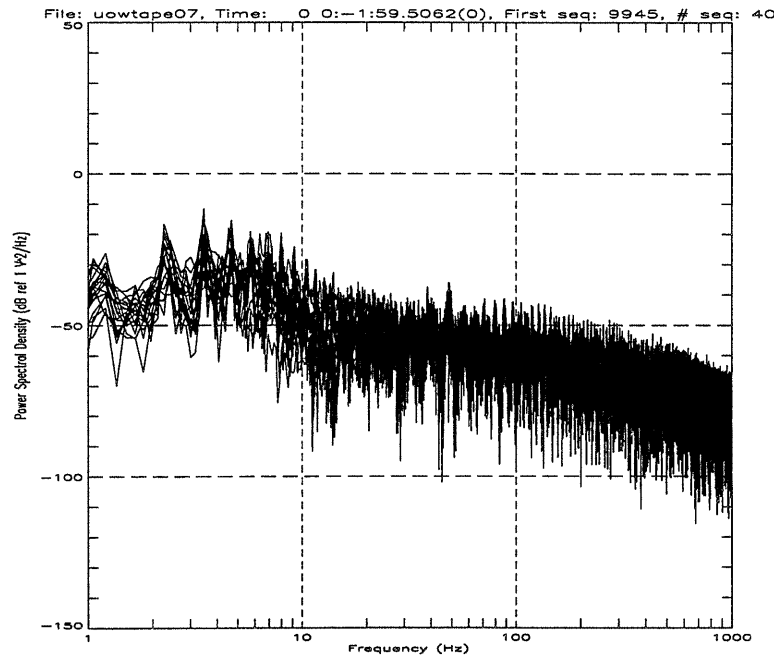
*Figure 4.2   The spectrum of shot 112 in run 1 from 1999 (21 vertical hydrophones, data
sequence 9945 – 9984, rectangular window).*

4.2   Simulations using OASP

The OASES module OASP was used for simulating the time responses. At first, the environmental model was set up according to the first-order geoacoustic model as presented in Figure 3.4 with five water layers. In addition, gradient water sound velocity and iso-velocity water layer were modelled. Automatic wave number sampling was selected (NW = - 1), in order to have full flexibility. The low frequency limit was set to 4 Hz, while the high frequency limit was set to 700 Hz. Since the time sampling was set to 0.0008 s, only frequencies up to 625 Hz was computed, see Appendix F. The standard input parameters are listed in Table 4.2. An example of the OASP input file is shown in Appendix F. The computations were time consuming due to the high frequency contents of the data, especially when simulating gradient sound velocity in one or more of the layers.

The different parameters in OASP were manually changed in order to study their sensitivity. It was soon discovered that the number of water layers could be reduced to three without any visible effects on the time responses. All three layers had constant sound velocity, with values as listed in Table 4.3. In order to take into account the bubble pulses, additional sources with reduced amplitudes were used as input. Based on the magnitude of the bubble pulses observed (rather than the theoretical values), the peak pressures of the shock pulse and first and second bubble pulses were set to $P_0 = 1$, $P_1/P_0 = 0.6$ and $P_2/P_0 = 0.4$, respectively. The observed second bubble pulse period of 227 ms, rather than the theoretical of 213 ms was used in the simulations (with a depth of 17.2 m). Figure 4.3 shows the simulated time responses using three sources and comparison with the measured data shows that both the first and second

bubble pulses in addition to the shock pulse are observed at the antenna. This is even clearer when simulating only the shock pulse, see Figure 4.4.

In summary, the comparisons between simulated and measured acoustic fields indicated:

- Four or five water layers may be reduced to three without any visible effects
- The substrate seems of no importance - if attenuation 0.7 dB/λ is used instead of 0.1 dB/λ, the pulse arrivals are perhaps earlier at the antenna
- Increasing the sediment attenuation has no visible effects
- Decreasing/increasing the sediment sound velocity gives minor changes in pulse forms and later/earlier pulse arrivals after some time
- Increasing sediment density gives minor changes in pulse forms after some time
- Decreasing the sound velocity in the water layer(s) gives later pulse arrivals and only minor changes in pulse forms
- Gradient sound velocity in the water layer(s) gives smoother pulse forms and no ripple around the pulse arrivals
- Iso-velocity water layer gives no ripple of the pulses, makes it possible to see additional pulse arrivals at the beginning of the time series
- Decreasing/increasing the water depth by a few meters (without changing receiver depths) gives earlier/later pulse arrivals
- Three sources are necessary to simulate the first 0.4 s of the acoustic field

OASP Parameter	Value
Source depth (mean of array), SD	17.2 m
Number of sources in array, NS	1, 2 or 3
Depth of first and last receiver, RD1 and RD2	115 m and 315 m
Number of receivers, NR	21
Minimum phase velocity, CMIN	1000 m/s
Maximum phase velocity, CMAX	10^8 m/s
Number of wavenumber samples, NW	-1 (automatic)
Number of time samples, NT	16384
Low frequency limit, F1	4 Hz
High frequency limit, F2	700 Hz (adjusted automatically)
Time sampling increment, DT	0.0008 s
First receiver range, RO	5.91 km

Table 4.2   Input parameters for OASP when simulating shot 112 in run 1 from 1999.

	Sound velocity	Thickness of layer	Attenuation	Density
Water layer 1	1488 m/s	30 m	0	1 g/cm³
Water layer 2	1473 m/s	245 m	0	1 g/cm³
Water layer 3	1465 m/s	44 m	0	1 g/cm³
Sediment	1800 m/s	37 m	0.5 dB/λ	2 g/cm³
Substrate	2400 m/s	Semi-infinite	0.1 dB/λ	2.2 g/cm³

Table 4.3   Standard OASP environmental parameters.

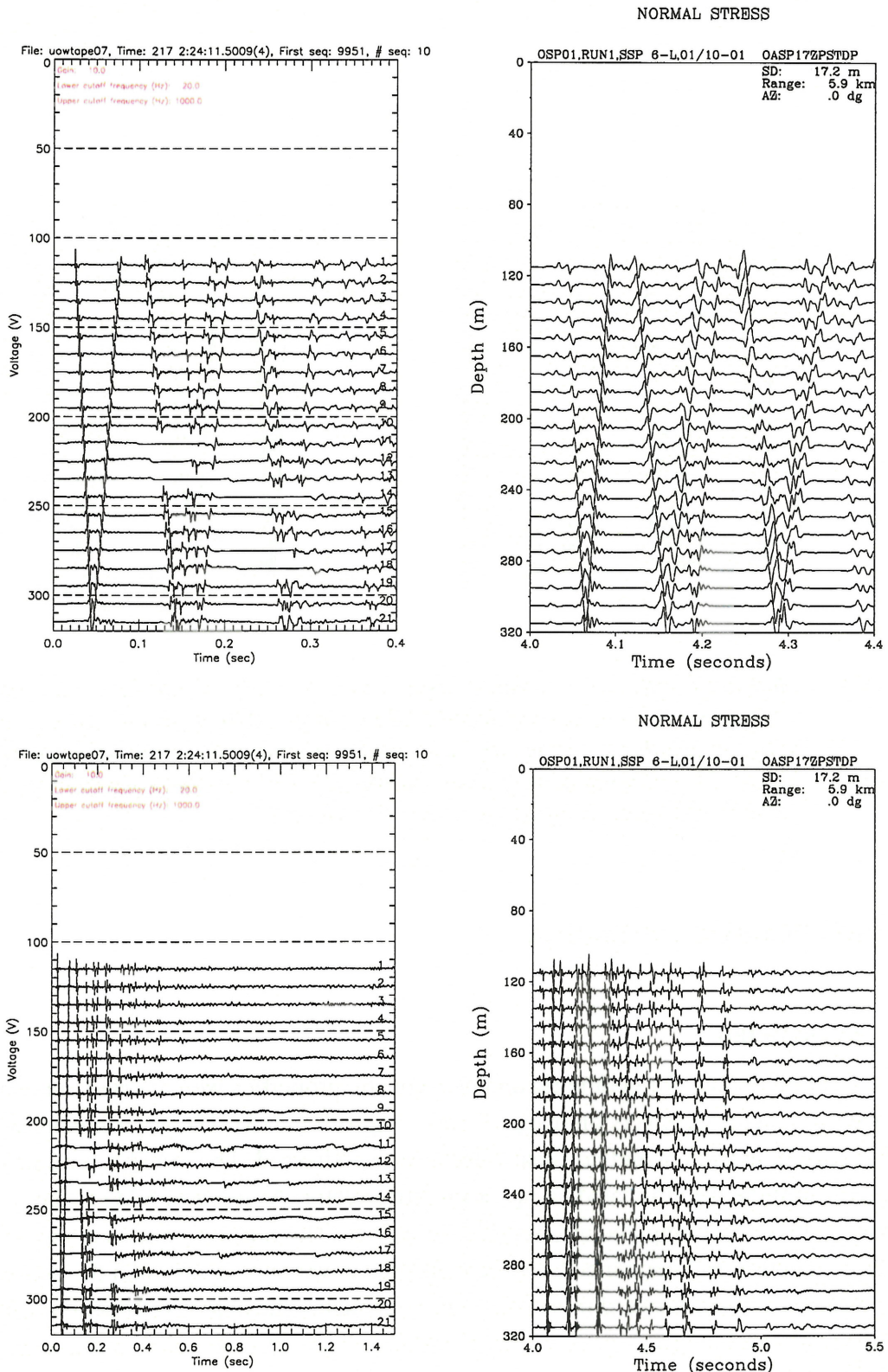Figure 4.3   *Measured (left) and simulated (right) pulse arrivals of shot 112. Three sources detonating at 0 ms, 126 ms and 227 ms, source depths 17.2 m, range 5910 m, water depth 319 m, upper hydrophone 115 m, six-layer model (vacuum, three iso-velocity water layers, 37 m thick sediment layer, substrate), 120 Hz source frequency, 4 – 625 Hz frequency integration. Time axes 400 ms (upper) and 1.5 s (lower).*
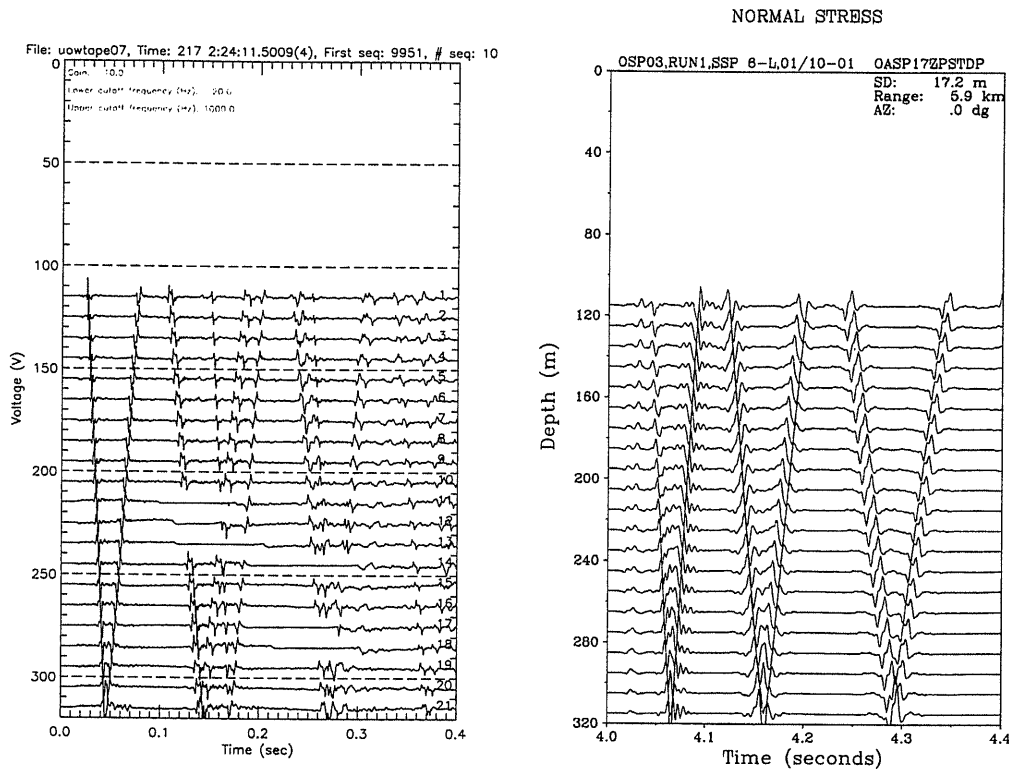
NORMAL STRESS

Figure 4.4   Measured (left) and simulated (right) pulse arrivals of shot 112. One source
detonating at 0 ms, source depth 17.2 m, range 5910 m, water depth 319 m,
upper hydrophone 115 m, six-layer model (vacuum, three iso-velocity water
layers, 37 m thick sediment layer, substrate), 120 Hz source frequency, 4 –
625 Hz frequency integration. Time axes 400 ms.

5   GEOACOUSTIC INVERSION

5.1   Background

Matched field inversions for geometric and geoacoustic properties were carried out using
SAGA (Seismo Acoustic inversion using Genetic Algorithms) (5). The environment was
assumed range independent and no shear effects were addressed. The OASES module OAST
was used to compute the simulated complex pressure vector. As input to SAGA, the
covariance matrix was computed at selected frequencies. The Bartlett processor was selected
as objective function and contained both the measured covariance matrix and the simulated
pressure vector from the forward modelling. For minimising the objective function, genetic
algorithms were used. During optimisation in SAGA, all obtained samples of the search space
are stored and may be used to estimate the a posteriori probability of each parameter. Based on
the a posteriori probability distribution, three estimates of the parameter are available from the
post-processor package POST (12)(13):

- best-of-all estimate, associated with the largest fit or lowest energy of the objective
  function (GA best)
- most-likeliy estimate, based on the peak of the distribution (GA ppd)

- mean estimate, based on the mean of the distribution (GA mean), the standard deviation of the distribution expressed as a fraction of the search interval of the parameter is also available (12)

The energy of the Bartlett processor is computed for all three cases. With perfect match between simulated and measured data, the energy is zero. If no match, the energy is 1 (assuming correct normalization of input data). If an inversion performs well the GA best, GA ppd and GA mean parameter estimates are approximately equal, and equivalent with the three energies. If the parameter estimates are quite different, probably multi-modal peaks are present in the *a posteriori* distribution or the parameter is not well determined, and it is a question which estimate describes the environment best. The GA mean Bartlett power in dB, which gives a measure of the fitness of the model is computed automatically in SAGA/POST (13). The GA best and GA ppd Bartlett power are easy to compute from the corresponding energy outputs. A Bartlett power of 0 dB means perfect match between simulated and measured data. The more negative value of the Bartlett power in dB, the worse the match is.

In addition to plotting the *a posteriori* distributions, simulated results are possible to compare with measured data across the array (for each hydrophone) in a MatLab plot with three panels:

- Left panel: The magnitudes of the measured and simulated (GA best) pressure vectors normalised. The normalization is given in Appendix G. When the covariance matrix is input, the measured pressure vector is estimated as the first eigenvector using singular value decomposition.
- Middle panel: The phases of the measured and simulated pressure vectors. The phases plotted are relative to the phase of the first hydrophone. The phases are unwrapped during plotting and if the phase difference between two following receivers are greater than 180°, then 360° is subtracted from the highest numbered receiver and if the phase difference is lower than -180°, then 360° is added to the phase of the highest numbered receiver.
- Right panel: The magnitude squared of the measured pressure vector compared with the Bartlett power across the array, as given in Appendix G. The sum of the Bartlett power across the array equals the GA best Bartlett power in dB.

Algorithms, normalization factors and plotting results are outlined in Appendix G.

Inversion of geometric and geoacoustic parameters were performed at 22.9 Hz, 40.4 Hz, 48.2 Hz, 48.9 Hz and 87.6 Hz. At first, single frequency inversion was intended, with a frequency between 10 – 20 Hz (11). Due to noise in the acoustic data, higher frequencies were preferred. The covariance matrix was computed using the interactive data language IDL for Windows (see Appendix G). At first, the frequency spectrum of 40 data sequences covering in total 6.6 s and starting about 1 s before the first pulse arrival was computed. Selecting a frequency, the covariance matrix was computed as the outer product of the complex pressure vector. The matrix was normalised by dividing with the norm of the pressure vector squared in order to have the Bartlett output energy equal 1 if no match, see Table 5.1.The refracted waves were not within the selected time window, due to noise these were anyhow not observable on the vertical antenna.

Each layer in the baseline model was described by depth, sound velocity, density, and attenuation. With five layers in addition to vacuum, the baseline model had 20 parameters. If the source-receiver range and source depth were allowed to vary, 22 parameters might be inverted. However, the following parameters were kept constant: the depth and density of the three water layers and the attenuation of all five layers. The remaining 11 parameters were inverted in six different models. In addition, the substrate was removed to study the effect on the water depth and sediment velocity. The receiver depths were assumed constant.

The parameter search spaces in SAGA were made wide in order to also have the possibility of non-plausible parameter estimates. Each search space was discretized into 128 values. With the given search spaces, the increments for the water depth, sediment thickness, sediment velocity and substrate velocity were 0.2 m, 0.4 m, 3 m/s and 13 m/s, respectively.

The number of forward modelling runs was between 2560 and 4096 dependent on the frequency, as higher frequency data required more computer time. Each population contained 64 individuals and the number of parallel population was usually 32 or 64. The crossover rate, reproduction size and mutation rate were as suggested by (14), namely 0.8, 0.5 and 0.05.

Frequency	Norm of pressure vector
22.9 Hz	0.00421
40.4 Hz	0.00705
48.2 Hz	0.01011
48.9 Hz	0.01058
87.6 Hz	0.00678

Table 5.1 *The norm of the pressure vector (21 hydrophones) at different frequencies. The frequency spectrum was computed from 40 data sequences covering in total 6.6 s and starting about 1 s before the first pulse arrival.*

5.2 Results and discussion

5.2.1 Single frequency inversion at 48.9 Hz

When keeping the parameters as in the baseline model, the GA best Bartlett power was −7.86 dB. The difference between measured and simulated pressure vector was large as seen in Figure 5.1 and the Bartlett power across the array was almost flat.

In model 1 the total water depth, sediment thickness, sediment sound velocity and substrate sound velocity were inverted. The results are plotted in Figure 5.2. The coherence between measured and simulated data was higher than for the baseline model. For the four bottom hydrophones there was apparently a difference in phase. This was however mostly due to the plotting. A phase difference of 360° is in fact no phase difference, since this could be due to one graph being unwrapped differently from the other graph. For the bottom hydrophone the phase of the measured pressure vector was -347°, while the phase of the simulated pressure vector was 18° or -342°. The GA best estimated parameters were 328.1 m, 32.5 m, 1610 m/s and 2265 m/s. The estimated water depth was 9 m deeper than in the baseline model. However, the value was consistent with the average water depth between the receiver and source position

(326 m). Both the sediment thickness and sediment velocity were less than in the baseline model, while the fraction was approximately unchanged. The substrate sound velocity was about 125 m/s lower than expected from the closest WABR measurement (no 5), see Section 3.1. The GA best Bartlett power increased from −7.86 dB to −1.43 dB. The results are listed in Table 5.2.

In addition to optimising the parameters mentioned above, inversion for the sound velocity in the three water layers was carried out in model 2. When each of the search bands was from 1450 m/s − 1490 m/s, the resulting parameter estimates were non-plausible. However limiting the search bands and the inversion results were quite well, see Figure 5.3. The sound velocity estimates were only 2 - 4 m/s below the baseline values. The GA best Bartlett power increased only from −1.43 dB to −1.42 dB. The GA best estimated parameters for water depth, sediment thickness, sediment velocity and substrate velocity were approximately the same as in model 1.

In model 3 the source-receiver range and the source depth were free to vary up to ± 100 m and ± 10 m respectively from the baseline values. The GA best Bartlett power increased considerably, from −1.43 dB to −0.83 dB. However, the parameter estimates for source depth was close to the lower search band (7 m), see Figure 5.4. Since the nominal detonation depth was 18 m and the estimated depth computed from the measured bubble pulse period was 17.2 m, an estimated inversion depth of 7 m or shallower seemed not plausible. The source-receiver range was not well determined. The GA best parameter estimate was 5.84 km, which was 70 m shorter than the true range. The GA best estimated parameters for water depth, sediment thickness, sediment velocity and substrate velocity were 326.3 m, 32.9 m, 1620 m/s and 2253 m/s, respectively.

Since the sediment thickness and sediment velocity in the first-order geoacoustic model were proportional, a shape function was introduced in model 4 to link these two parameters and reduce the overall number of parameters in the inversions. The sediment thickness was set to be 0.02055 multiplied with the velocity. Thus a velocity of 1800 m/s would give a sediment thickness of 37 m, in accordance with the first-order geoacoustic model. The estimate of the shape function coefficient was equal to the estimated sediment velocity. Figure 5.5 shows the inversion results. The Bartlett power decreased only 0.01 dB compared with not using the shape function (see model 1). The GA best estimated parameters for water depth, sediment thickness, sediment velocity and substrate velocity were 328.1 m, 33.2 m, 1613 m/s and 2309 m/s, respectively. Hence, linking these two parameters had only minor influence on the parameter estimates.

If not inverting the substrate velocity (model 5), only the sediment parameters were influenced, as shown in Figure 5.6. The parameter estimates for water depth, sediment velocity and sediment thickness were 328.1 m, 1613 m/s and 33.7 m respectively. The GA best Bartlett power was −1.46 dB.

When optimising the sediment and substrate densities in addition to water depth, sediment and substrate velocities and sediment thickness (model 6), the Bartlett Power increased from −1.43 dB to −1.40 dB. Figure 5.7 shows the results. The GA best parameter estimates for the sediment density was 2.15 g/cm^3, which was 0.15 g/cm^3 higher than the baseline value. The

GA best estimate for the substrate velocity was 2.80 g/cm^3, which was considerable higher than expected. The GA best estimated parameters for water depth, sediment thickness, sediment velocity and substrate velocity are listed in Table 5.2.

To conclude, all inversions at this frequency indicated a water depth of around 326 - 328 m, and a sediment layer thickness of 32 – 34 m. The sediment sound velocity varied only minor, between 1607 - 1620 m/s. A sediment velocity of down to 1600 m/s indicated that the signals only "saw" the upper part of the sediment. A sediment velocity of 1800 m/s as presented in the baseline model was implicit stating the average velocity over the whole layer. The parameter estimates for the substrate velocity varied much more, between 2228 – 2309 m/s. Hence the inversion results implied that substrate layer was of minor importance to the acoustic propagation.

In order to study the effect of the substrate layer, the layer was removed in model 7 and 8, and the sediment layer was made half-space. In model 7 the sound velocities in the three water layers, sediment velocity and water depth were inverted. Figure 5.8 shows the results and the parameter estimates are listed in Table 5.3. The GA best Bartlett power was -1.93 dB, which was a considerable decrease in match between simulated and measured data. The parameter estimate for the sediment velocity increased to 1670 m/s, which was as expected since the higher velocity substrate layer of 2400 m/s was removed. The parameter estimate for the water depth was 328.9 m and in coherence with earlier depth estimates. If only inverting the water depth and sediment velocity (model 8), the parameter estimates became 330.6 m and 1686 m/s respectively, see Figure 5.9. The GA best Bartlett power was -2.04 dB. Since the Bartlett powers decreased using five layers in the environmental model instead of six layers, the six-layer model was used in the source localization.

	Baseline	Model 1	Model 2	Model 3	Model 4	Model 5	Model 6
Water speed layer 1 (m/s)	1488		1484				
Water speed layer 2 (m/s)	1473		1471				
Water speed layer 3 (m/s)	1465		1461				
Water depth (m)	319	328.1	327.8	326.3	328.1	328.1	328.4
Sediment thickness (m)	37	32.5	32.5	32.9	*33.2*	33.7	31.3
Sediment speed (m/s)	1800	1610	1607	1620	*1613*	1613	1610
Sediment density (g/cm^3)	2.0						2.15
Substrate speed (m/s)	2400	2265	2265	2253	2309		2228
Substrate density (g/cm^3)	2.2						2.80
Source depth (m)	17.2			<7			
Range (km)	5.91			5.84			
Bartlett power (dB)	-7.86	-1.43	-1.42	-0.83	-1.44	-1.46	-1.40

Table 5.2   GA best parameter estimates and Bartlett power for different six-layer models (vacuum, three water layers sediment layer and substrate layer). The six models are described in the text. The parameters of the values in cursive were linked.

	Baseline	Model 7	Model 8
Water speed layer 1 (m/s)	1488	1472	
Water speed layer 2 (m/s)	1473	<1460	
Water speed layer 3 (m/s)	1465	1452	
Water depth (m)	319	328.9	330.6
Sediment speed (m/s)	1800	1670	1686
GA best Bartlett power (dB)	-8.65	-1.93	-2.04

Table 5.3   *GA best parameter estimates for five-layer models (vacuum, three water layers and sediment layer). The two different models are described in the text.*

Results from data newbase2
File: l:\neptun\user\majola1131_99\aeg\el48\newbase2; Date: 02-Dec-2001
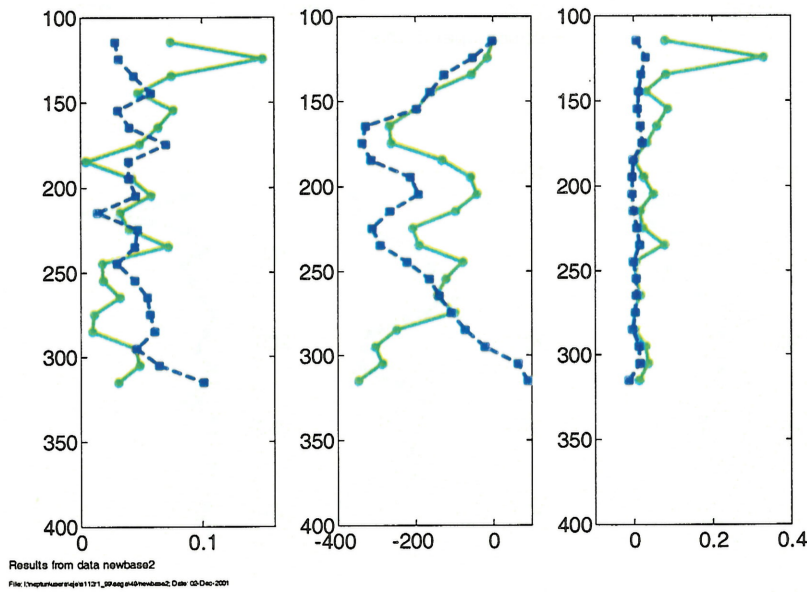
Figure 5.1   *Comparison of baseline model and measured data at 48.9 Hz. The magnitudes of the measured (green, solid line with circles) and simulated (blue, dashed line with squares) pressure vectors normalised are shown in the right panel, in the middle panel the phases of the two vectors are shown (relative to the phases of the top hydrophone), and left is the magnitude squared of the measured pressure vector (normalised with the norm squared) compared with the Bartlett power across the array. The Bartlett power of the baseline model at this frequency was −7.86 dB.*

Depth of layer (m)

Layer thickness (m)

P-sound speed (m/s)

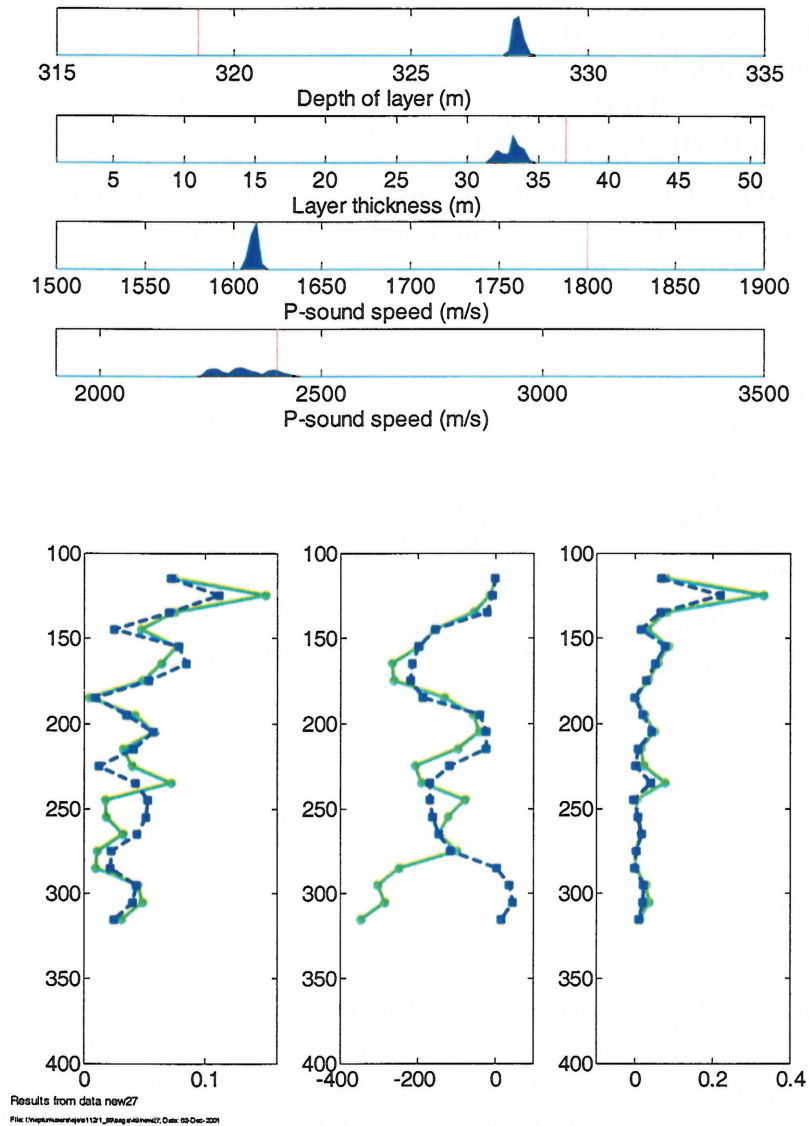P-sound speed (m/s)

Results from data new27

Figure 5.2   *Inversions results for water depth, sediment thickness, sediment velocity and substrate velocity at 48.9 Hz. Upper: The a posteriori distributions. Lower: Comparison of measured and simulated results across the array.*
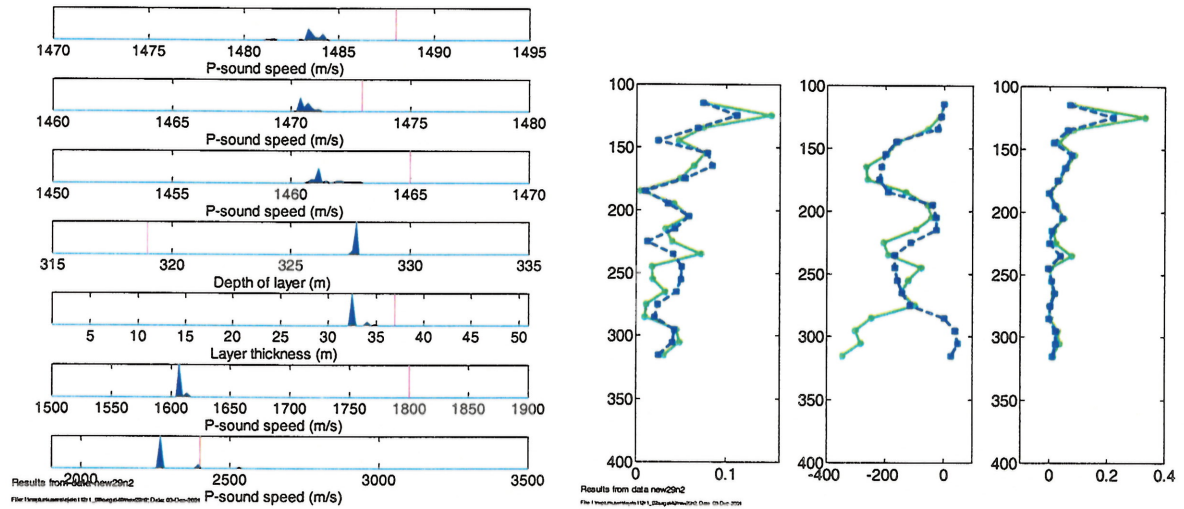*GA best: -1.43 dB, GA mean: -1.45 dB.*

Figure 5.3   Inversions results for the seven parameters at 48.9 Hz. Upper: The a posteriori distributions. Lower: Comparison of measured and simulated results across the array. GA best: -1.42 dB, GA mean: -1.42 dB.
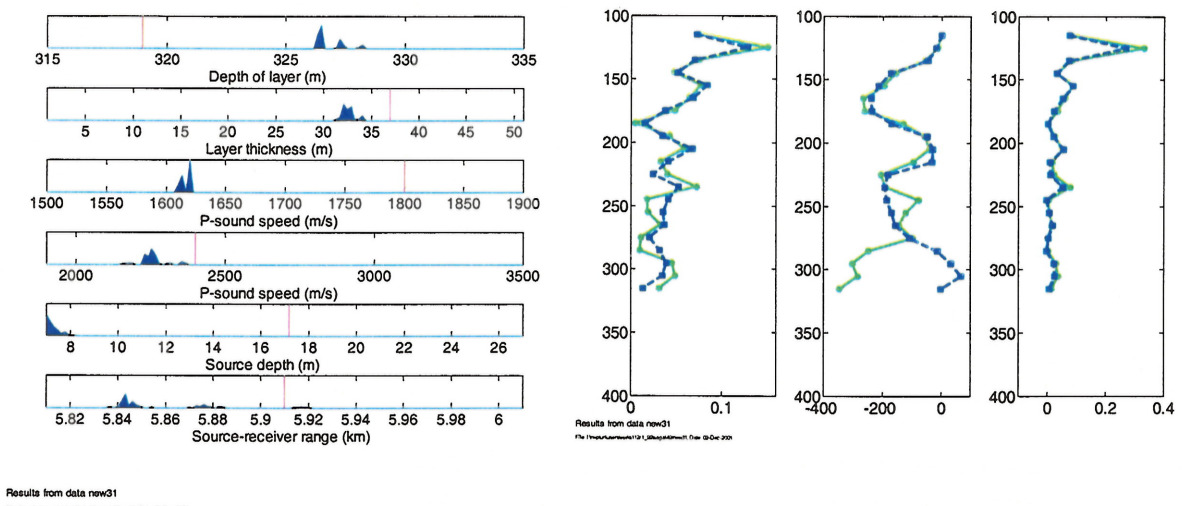

Figure 5.4   Inversions results for six parameters at 48.9 Hz. The source depth and range were allowed to vary slightly in the inversion. Upper: The a posteriori distributions. Lower: Comparison of measured and simulated results across the array. GA best: -0.83 dB, GA mean: -0.84 dB.
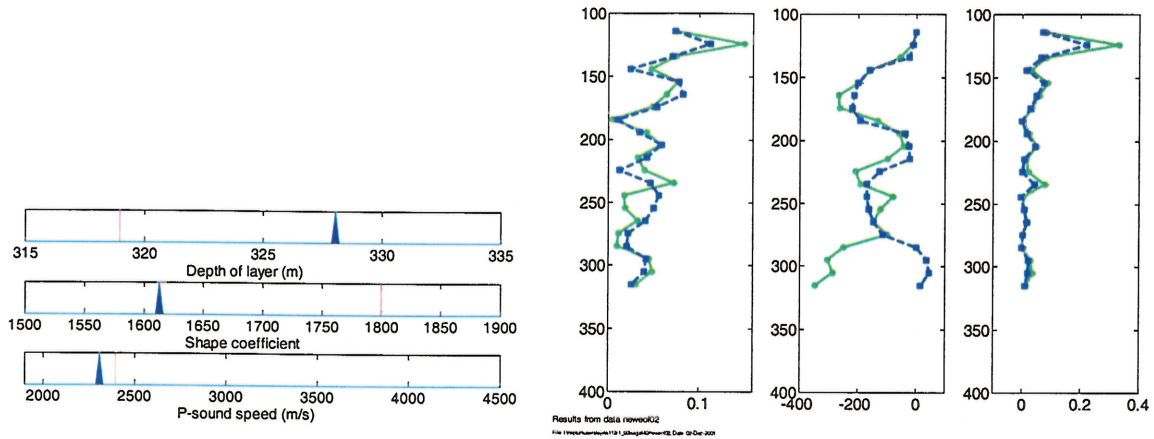
28

Figure 5.5   *Inversions results for three parameters at 48.9 Hz. The sediment sound velocity and the sediment thickness were linked together in the shape function. Upper: The a posteriori distributions. Lower: Comparison of measured and simulated results across the array. GA best: -1.44 dB, GA mean: -1.44 dB.*
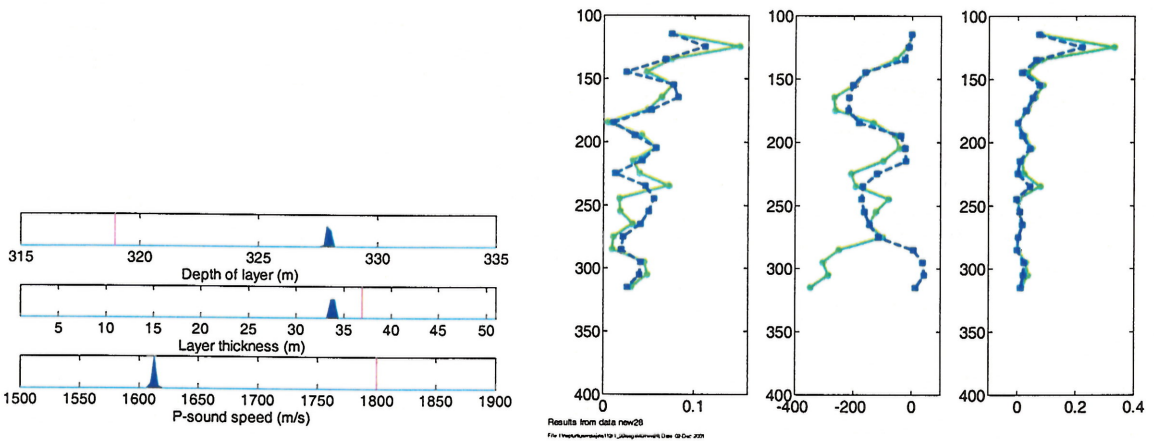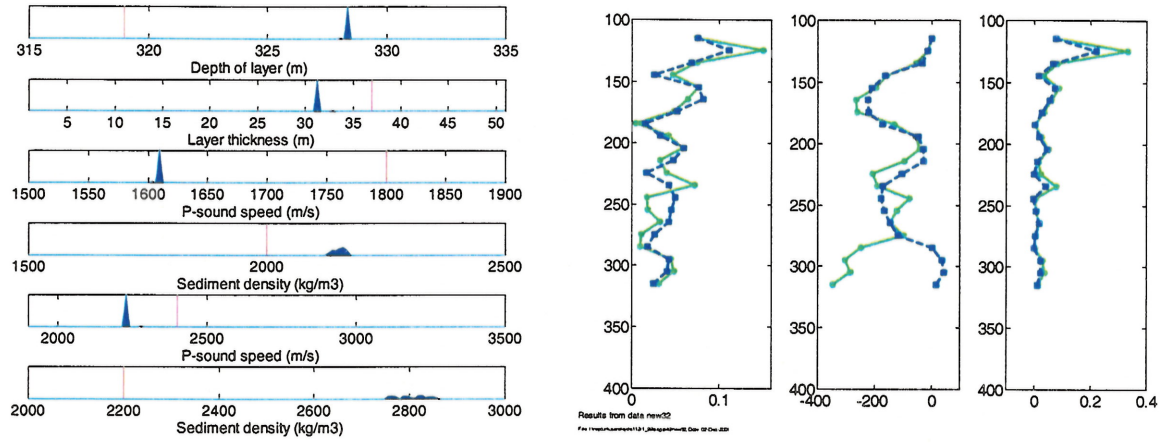

Figure 5.6   *Inversions results for three parameters at 48.9 Hz. The substrate velocity was not inverted (assumed not sensitive). Upper: The a posteriori distributions. Lower: Comparison of measured and simulated results across the array. GA best: -1.46 dB, GA mean: -1.45 dB.*

Figure 5.7 Inversions results for six parameters at 48.9 Hz. The sediment and substrate densities were optimised in addition to the water depth, sediment thickness, sediment velocity and substrate velocity. Upper: The a posteriori distributions. Lower: Comparison of measured and simulated results across the array. GA best: -1.40 dB, GA mean: -1.40 dB.
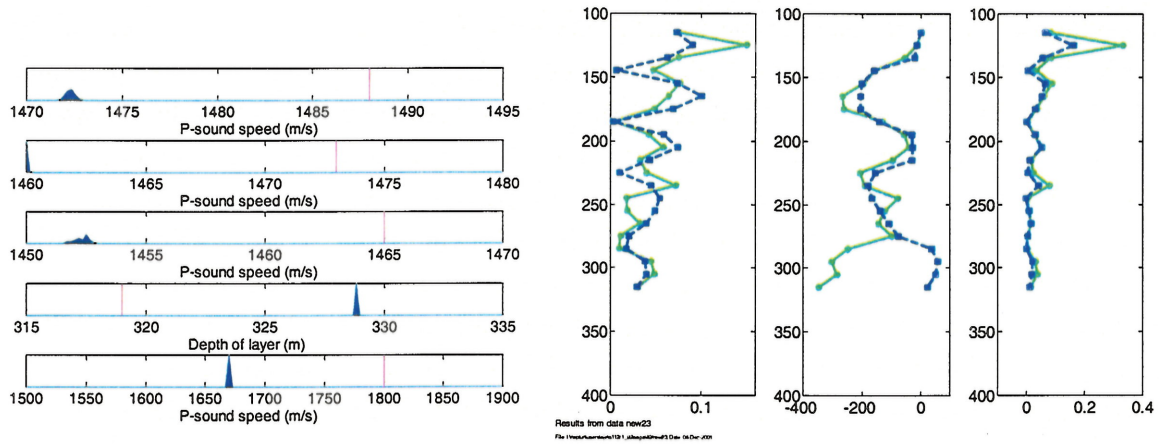
Figure 5.8 Inversions results for five parameters at 48.9 Hz. The model consisted of five layers instead of six, i.e. the substrate was removed. Upper: The a posteriori distributions. Lower: Comparison of measured and simulated results across the array. GA best: -1.93 dB, GA mean: -1.93 dB.
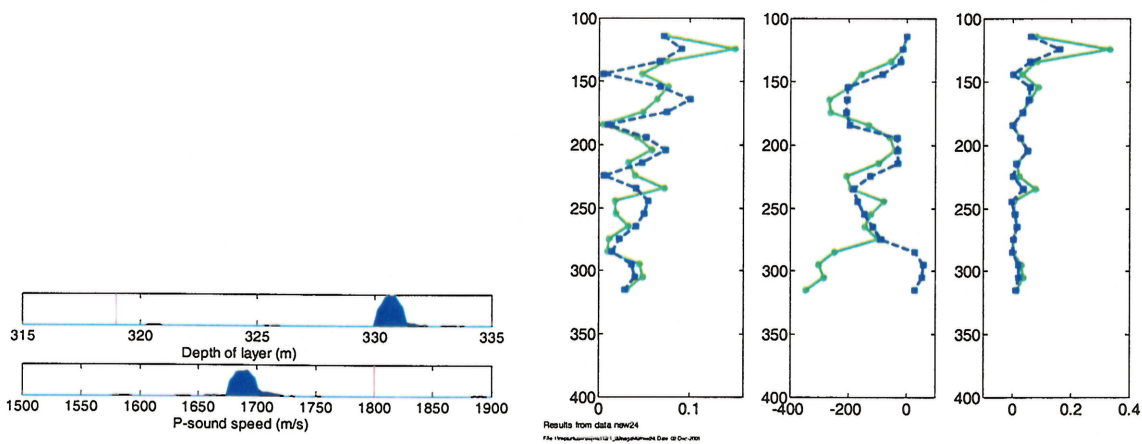
Figure 5.9 *Inversions results for two parameters at 48.9 Hz. The model consisted of five layers instead of six – the substrate was removed. Upper: The a posteriori distributions. Lower: Comparison of measured and simulated results across the array. GA best: -2.04 dB, GA mean: -2.05 dB.*

Using option C1 in SAGA correlation analysis was carried out at 48.9 Hz, see Figure 5.10. From the contour plots the sensitivity of each parameter is shown (assuming the other parameters were equal to the baseline values). The vertical axis gives the relative value of the objective function expressed in dB. The water depth seemed to be strongly correlated with the sediment velocity (a), and partly with the sediment thickness (for thin sediment layers) (b). For thick sediment layers (above 20 m) the water depth was not sensitive for the sediment thickness. The water depth was not correlated with the substrate velocity (c). These results indicated that the substrate was not important if the sediment thickness was above 20 m, which was in agreement with earlier interpretations. The correlation plot between sediment velocity and substrate velocity showed an area of higher energy for substrate velocity between 1900 – 2600 m/s and sediment velocity between 1500 – 1550 m/s (d). The peaks observed in the correlation plot between the sediment velocity and sediment thickness (e) indicated some correlation, but not as strong as expected. The last plot showed that the sediment thickness was not sensitive for the substrate velocity (f), except maybe for low substrate velocity, in which case the contrast between the sediment and substrate would be small. Correlation plots for the water velocities showed low sensitivity for these parameters in the given search band, and is not shown here.
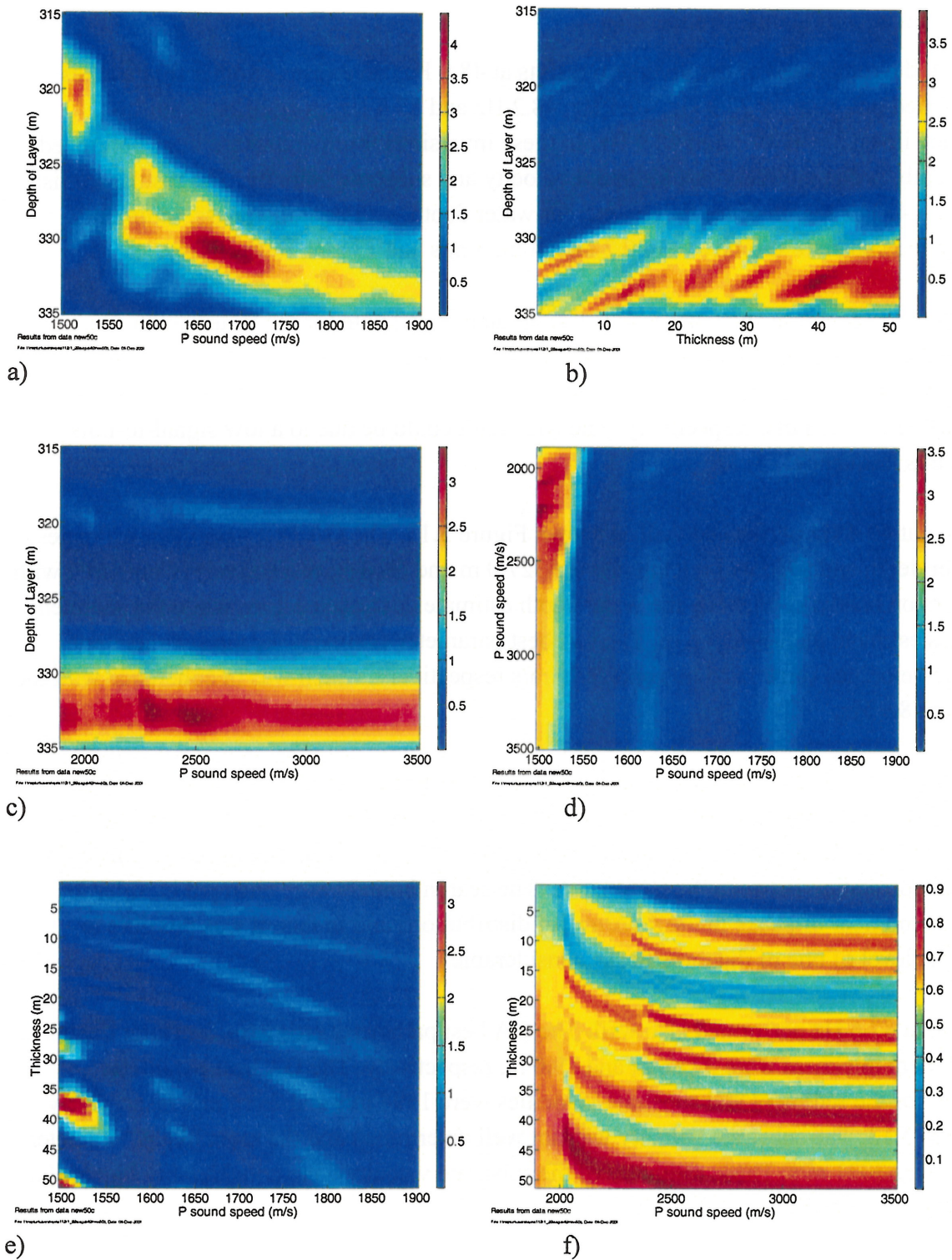
Figure 5.10 Correlation analysis using option C1 in SAGA. a) Water depth vs sediment velocity, b) water depth vs sediment thickness, c) water depth vs substrate velocity, d) sediment velocity vs substrate velocity, e) sediment velocity vs sediment thickness and f) substrate velocity vs sediment thickness.

5.2.2 Inversions at other frequencies

To check the robustness of the inversion results at 48.9 Hz, inversions at other frequencies were carried out, namely 22.9 Hz, 40.4 Hz, 48.2 Hz and 87.6 Hz, in addition to multi-frequency inversion at 48.2 and 48.9 Hz. In these inversions four parameters were optimized: water depth, sediment thickness, sediment velocity and substrate velocity. The results are listed in Table 5.4. The search space increments for water depth, sediment thickness, sediment velocity and substrate velocity were 0.2 m, 0.4 m, 3 m/s and 13 m/s, respectively.

Inversion at 22.9 Hz was not successful. The parameter estimate for the water depth was 319 m, which was equal to the receiver depth. The parameter estimate for the sediment velocity was close to the lower search band. The GA best and GA mean Bartlett power were – 4.30 dB and – 5.78 dB, respectively. The bad result could be due to a low signal-to-noise ratio at this frequency.

Inversion at 40.4 Hz performed well as shown Figure 5.11. The GA best parameter estimates for water depth and sediment thickness were 327.0 m and 36.0 m, respectively. Compared with the inversion results at 48.9 Hz, the water depth estimate decreased 1.1 m, while the sediment thickness estimate increased 3.5 m. The GA best parameter estimates for the sediment and substrate velocities were 1626 m/s and 2190 m/s respectively, which was in coherence with the results at 48.9 Hz.

Inversion at 48.2 Hz gave multi-modal peaks for the sediment parameters and water depth, while the substrate velocity was not well determined, see Figure 5.12. The GA best Bartlett power was 1.68 dB, while the GA mean Bartlett power was 3.70 dB. The multi-modal peaks indicated correlation between the parameters. The search bounds were changed in order to reduce the number of peaks in the *a posteriori* distributions and in fact, it was possible to reduce the level of one of the three peaks considerable

Inversion at 87.6 Hz performed also well. The GA best parameter estimates for water depth and sediment thickness were 327.6 m and 29.0 m, respectively. The GA best parameter estimates for the sediment and substrate velocities were 1594 m/s and 2946 m/s respectively, see Figure 5.13. The substrate velocity was not well determined and the most likely parameter estimate was 3021 m/s. These estimates of the substrate velocity were considerably higher than in the other inversions.

In order to investigate if the robustness became higher using multi frequency inversion, 48.2 Hz was used in addition to 48.9 Hz. The inversion results are plotted in Figure 5.14. The GA mean Bartlett powers (one for each frequency) were –1.85 dB and –1.65 dB. The GA best parameter estimates for the sediment and substrate sound velocities were 1617 m/s and 2958 m/s, respectively. Again, the substrate velocity estimate was high. The GA best parameter estimate for the water depth was 328.1 m. The estimated thickness of sediment layer was 36.0 m, which was thicker than expected from the single frequency inversions.

	48.9 Hz	40.4 Hz	48.2 Hz	87.6 Hz	48.2 Hz and 48.9 Hz
Water depth (m)	328.1	327.0	Multi-	327.6	328.1
Sediment thickness (m)	32.5	36.0	modal	29.0	36.0
Sediment speed (m/s)	1610	1626	peaks	1594	1617
Substrate speed (m/s)	2265	2190		2946	2958
GA best Bartlett power (dB)	-1.43	-1.82		-2.87	-1.85 (48.2 Hz) -1.65 (48.9 Hz)

Table 5.4   *GA best parameter estimates for six-layer models at different frequencies. The summation over frequency for multi-frequency inversion was incoherent. The search space increments for water depth, sediment thickness, sediment velocity and substrate velocity were 0.2 m, 0.4 m, 3 m/s and 13 m/s, respectively.*
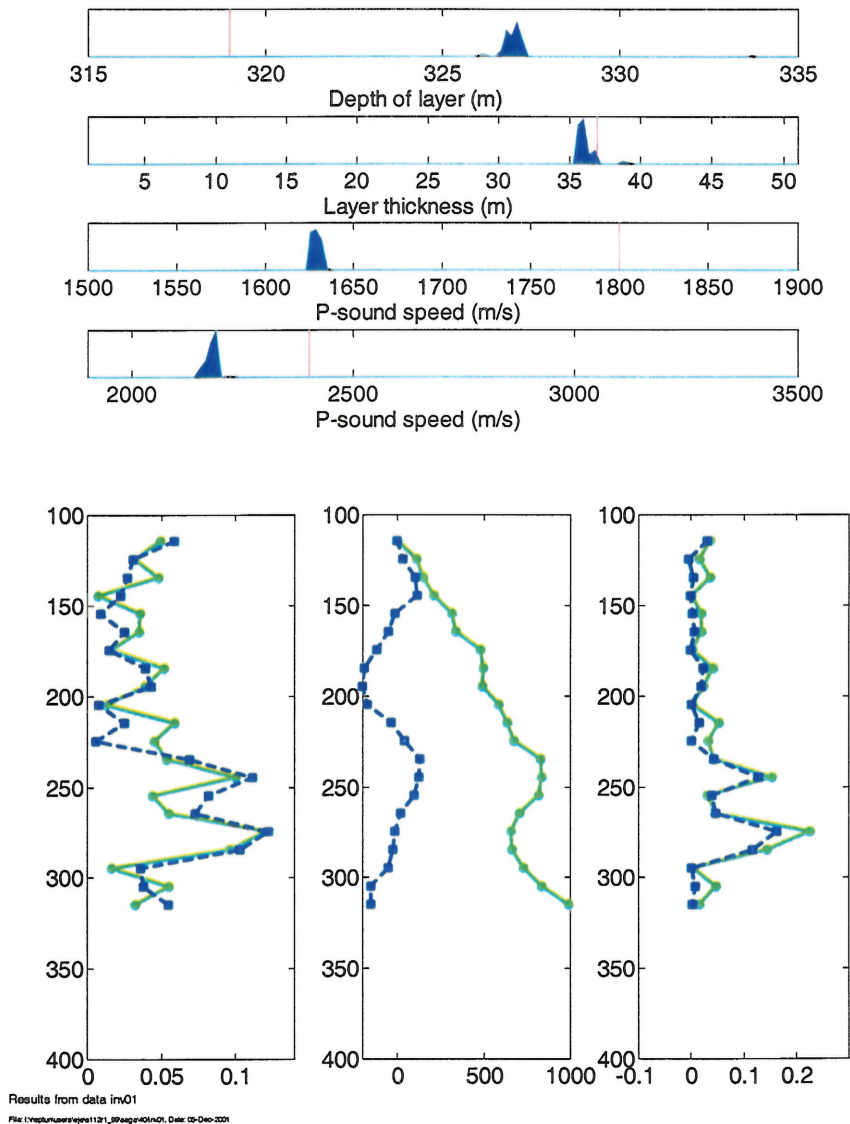
Figure 5.11   *Inversions results for three parameters at 40.4 Hz. Upper: The a posteriori distributions. Lower: Comparison of measured and simulated results across the array. GA best: -1.82 dB, GA mean: -1.97 dB.*

Figure 5.12 Inversions results for three parameters at 48.2 Hz. Upper: The a posteriori distributions. Lower: Comparison of measured and simulated results across the array. GA best: -1.68 dB, GA ppd: -5.67, GA mean: -3.70 dB.

Figure 5.13   *Inversions results for four parameters at 87.6 Hz. Upper: The a posteriori distributions. Lower: Comparison of measured and simulated results across the array. GA best: -2.87 dB, GA mean: -2.86 dB.*
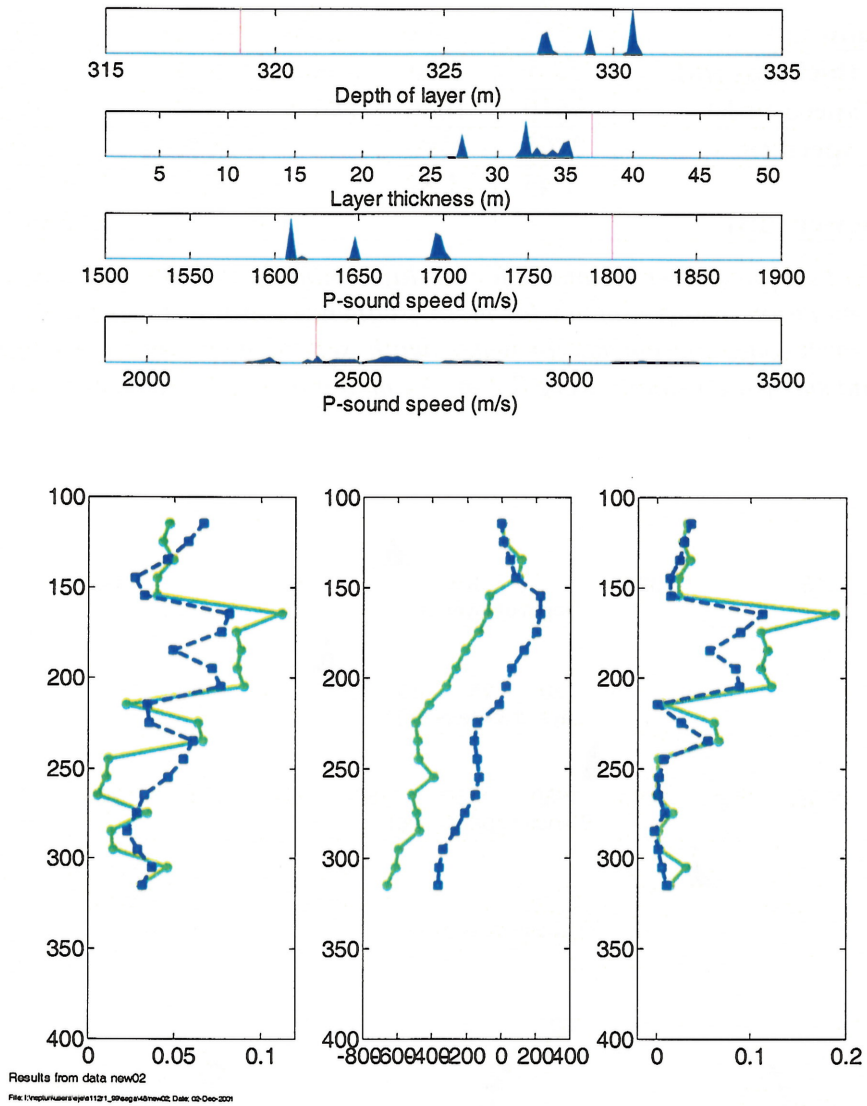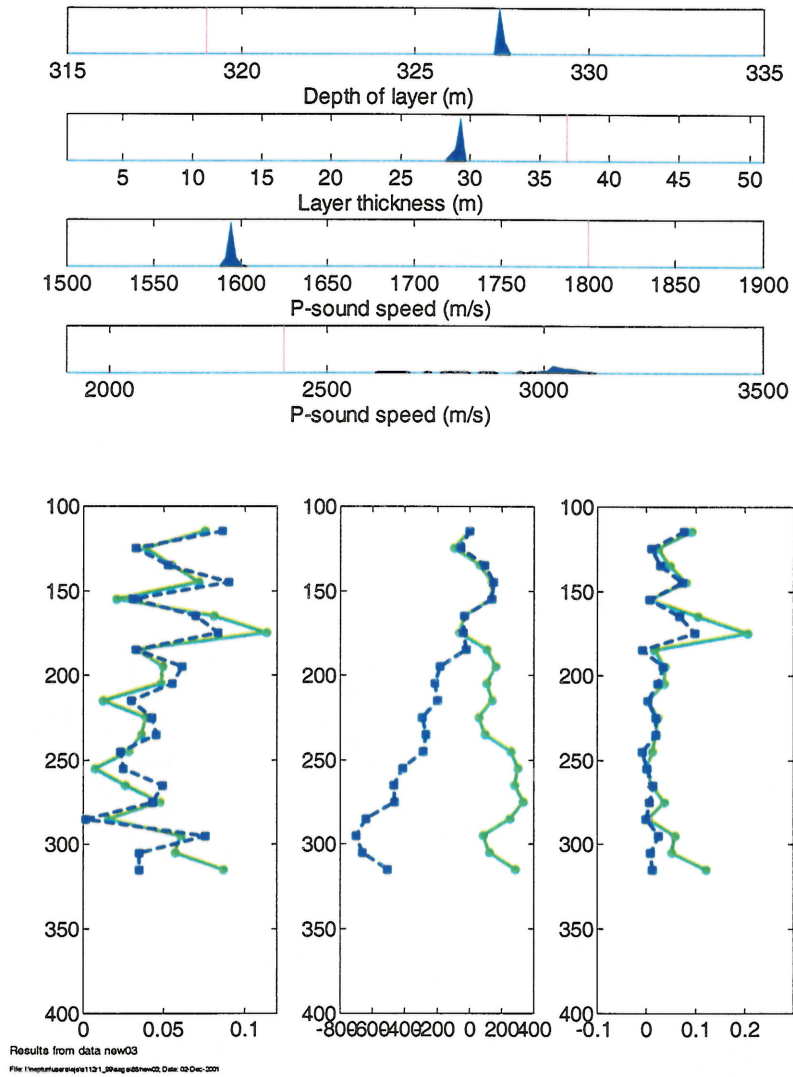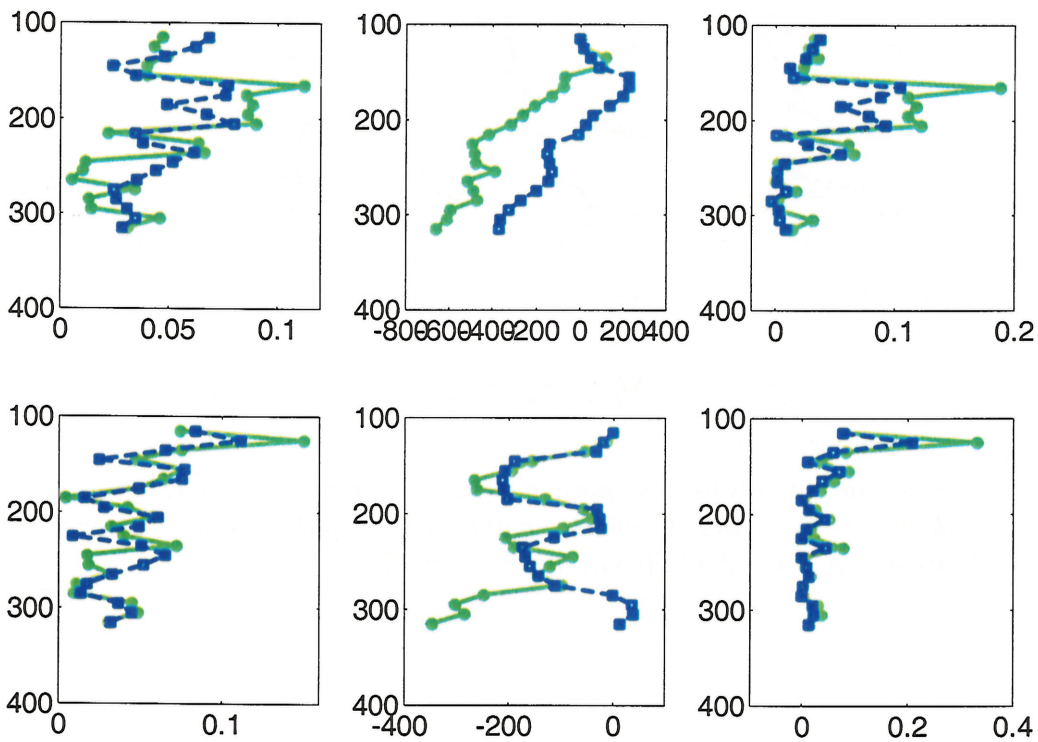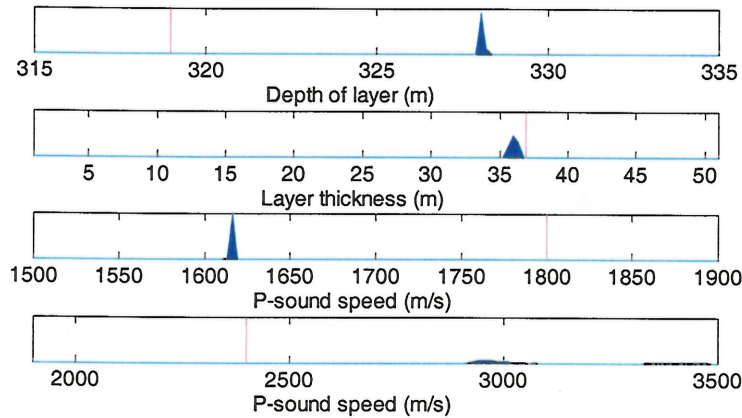
Figure 5.14   *Inversions results for three parameters at 48.2 Hz and 48.9 Hz. The sediment sound velocity and the sediment thickness were linked together in a shape function. Upper: The a posteriori distributions. Lower: Comparison of measured and simulated results across the array. GA mean (48.2 Hz): -1.85 dB, GA mean (48.9 Hz): -1.65 dB.*

6 SOURCE LOCALIZATION

Source localization (matched field procedures for localization) was carried out at different frequencies. SAGA and the OASES module OAST were used in a similar way as during the inversions. In localization the geoacoustic and geometric parameters were assumed known, and the acoustic field was inverted with respect to source depth and source-receiver range. Both *a posteriori* distributions and ambiguity surfaces were computed.

Localization was carried out both for the baseline model and the baseline model with GA estimated parameters at 48.9 Hz, that was assuming a water depth of 328.0 m, a sediment thickness of 32.0 m and a sediment velocity of 1610 m/s and keeping the other parameters as in the baseline model. The source-receiver range search band was set from 1 km to 20 km with 128 discrete values. Hence the range increment was $\Delta r = 150$ m. Near the true range value of 5.910 km the following range estimates were possible: 5.79 km, 5.94 km (closest) and 6.09 km. The source depth search band was set from 1 m to 315 m, which was approximately the entire water column. The depth parameter had 128 discrete values and the depth increment was hence $\Delta d = 2.5$ m. Near the true depth value of 17.2 m the following depth estimates were possible: 13.4 m, 15.8 m, 18.3 m (closest) and 20.8 m.

The ambiguity surfaces showed the objective function versus range and depth. The energy of the objective function was scaled relative to the minimum or maximum energy in the computations, and expressed in dB. When computing the ambiguity surfaces, the range parameter was discretized into 128 values with a resolution of $\Delta r = 150$ m (as for the *a posteriori* distributions), while the depth parameter was discretized into 64 values with a resolution of $\Delta d = 5.0$ m. Arrows above the ambiguity surfaces plotted in the report mark the peaks in the *a posteriori* distributions. Mainly the GA ppd estimates are presented and discussed, the reason will be clear at the end of the chapter.

The results of source localization at 48.9 Hz based on the baseline model is shown in Figure 6.1. The parameter estimate for the source-receiver range was 8.78 km, which was about 2.9 km higher than true (baseline) value. The GA ppd parameter estimate for the source depth was 18.3 m, which was the closest value possible to the true value. The Bartlett power was only –2.67 dB.

Using the baseline model with GA estimated parameters at 48.9 Hz, the source localization seemed promising as shown in Figure 6.1. Both source depth and source-receiver range was well determined. The GA ppd parameter estimates for source depth was 23.3 m and the deviation from the baseline model was only 6.1 m. The GA ppd parameter estimates for range was 5.94 m, which was as close as possible to the true range value. The Bartlett power was surprisingly low (–2.84 dB) taken into consideration that the same covariance matrix was used both in inversion and localization (which itself was dubiously). Remembering that a Bartlett power of –0.8 dB was obtained when allowing the depth and range to be free to vary ± 10 m and ± 100 m respectively, a higher Bartlett power was expected. The low match could be due

to 1) the environmental parameters were kept constant during the localization and/or 2) the resolution in range was too large.

The ambiguity surfaces are plotted in Figure 6.2. The peaks in the *a posteriori* distributions were easily identified in the surface plots as the strongest peaks (marked with arrows). Most of the peaks in the ambiguity surface for the baseline model disappeared or diminished in the ambiguity surface for the baseline model with the GA estimated parameters at the same frequency. However one peak at about 19 km increased in strength and could be mistaken as the source.

Source localization at 40.4 Hz gave multimodale peaks in the *a posteriori* distributions, both for the baseline model and the baseline model with GA estimated parameters at 48.9 Hz, see Figure 6.3. None of the peaks in the *a posteriori* distribution for the range parameter were at the true range. The source depth was not well determined in any of the models.

Localization at 48.2 Hz gave two peaks in the *a posteriori* distributions for the baseline model as shown in Figure 6.4. The largest peak for the range parameter was at 10.9 km, but there was also a second peak at 5.0 km, which gave the best fit between the simulated and measured data. For the baseline model with GA estimated parameters at 48.9 Hz, there was only one peak at 5.94 km, which was as close as possible to the true range. The depth estimate was 31 m. The ambiguity surfaces are plotted in Figure 6.5. The peaks from the *a posteriori* distributions were easily identified as the strongest peaks. Again many of the peaks in the ambiguity surface for the baseline model disappeared or diminished in the ambiguity surface for the baseline model with the GA estimated parameters at 48.9 Hz.

Figure 6.6 shows the *a posteriori* distributions for source localization at 87.6 Hz. For the baseline model the parameter estimates were well determined. The GA ppd depth estimate was 16 m and very close to the truth. However, the GA ppd parameter estimate for range was 11.6 km, which was about 5.7 km from the true value. For the baseline model with GA estimated parameters at 48.9 Hz, the GA best, GA ppd and GA mean parameter estimates for source-receiver range were quite different, even of there was a clear peak in the *a posteriori* distribution. The GA ppd (most likely) range estimate was 5.94 km, which was as close as possible to the true value. The GA best range estimate was 3.1 km and the GA mean range estimate was 9.4 km. The GA best depth estimate was far from the true value (179 m), while the GA ppd depth estimate was 18.3 m, which was as close as possible to the true value. The ambiguity surfaces are plotted in Figure 6.7 and confirm the results. The highest peak in the ambiguity surface was located at 3.1 km range and 179 m depth, and was identified as giving the best match/lowest energy of the Bartlett processor. The peak at 5.9 km range and 18 m depth was weaker in energy. Hence, in this inversion the GA best estimates were wrong, while the GA ppd estimates were as close as possible to the true solution. Consequently, from the ambiguity surface wrong conclusions may be drawn. Fortunately, the differences between the GA best and GA ppd parameter estimates were usually not so dramatic.

Using the covariance matrix at three frequencies 40.4 Hz, 48.2 Hz and 87.6 Hz as input in the source localization, the GA ppd parameter estimate for range was 7.3 km and for depth was close to the lower search band (1 m) as shown in see Figure 6.8. Using the baseline model with

GA estimated parameters at 48.9 Hz, the GA ppd parameter estimate for range was 5.94 km and for depth 26 m. The ambiguity surfaces are plotted in Figure 6.9.

To conclude, using a baseline model with GA estimated water depth, sediment thickness and sediment velocity at 48.9 Hz, the source-receiver range estimates were improved remarkable than using only the baseline model. While estimates of the source depth were within the correct water level for both models. Generally, there were many peaks in the ambiguity surface for the baseline model (even if the *a posteriori* distributions only have one peak each). The number of peaks was considerably reduced for the baseline model with GA estimated parameters at 48.9 Hz. However, the true peak may not be the strongest.

	48.9 Hz	**40.4 Hz**	**48.2 Hz**	**87.6 Hz**	**40.4 Hz, 48.2 Hz & 87.6 Hz**
Baseline model					
Range	8.8 km	Multi-modal peaks	10.9 km	11.6 km	7.3 km
Depth	18 m		<1 m	16 m	<1 m
Bartlett power	-2.7 dB		-3.7 dB	-4.3 dB	-6.1 dB
Baseline model with GA estimated parameters at 48.9 Hz					
Range	5.94 km	Multi-modal peaks	5.94 km	5.94 km	5.94 km
Depth	23 m		31 m	18 m	26 m
Bartlett power	-2.8 dB		-3.4 dB	-4.4 dB	-5.2 dB

Table 6.1   Source localization results. The GA ppd parameter estimates for source depth and source receiver range, and the GA ppd Bartlett power are listed. The true depth was 17.2 m and the true range was 5.91 km. The range increment was 150 m, and the depth increment was 2.5 m. With the given search bands and number of discrete values, the closest possible range and depth estimates were 5.94 km and 18 m, respectively.
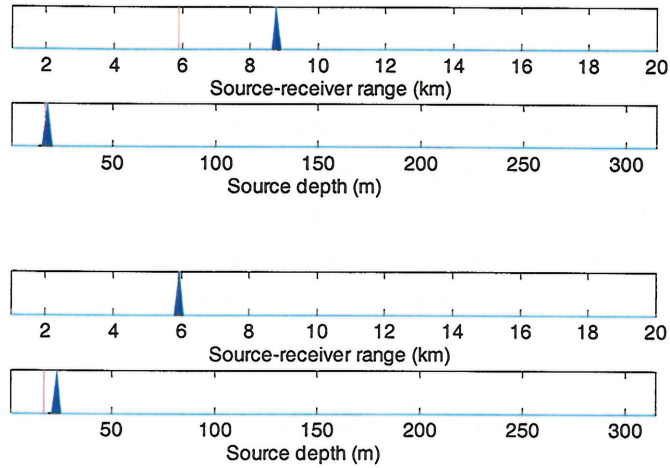
Figure 6.1   *Source localization at 48.9 Hz showing the a posteriori distributions. Upper: baseline model, GA best/ppd/mean: -2.67 dB. Lower: baseline model with GA estimated parameters at 48.9 Hz (D=328 m, d=32 m, c1=1610 m/s), GA best/ppd/mean: -2.84 dB.*
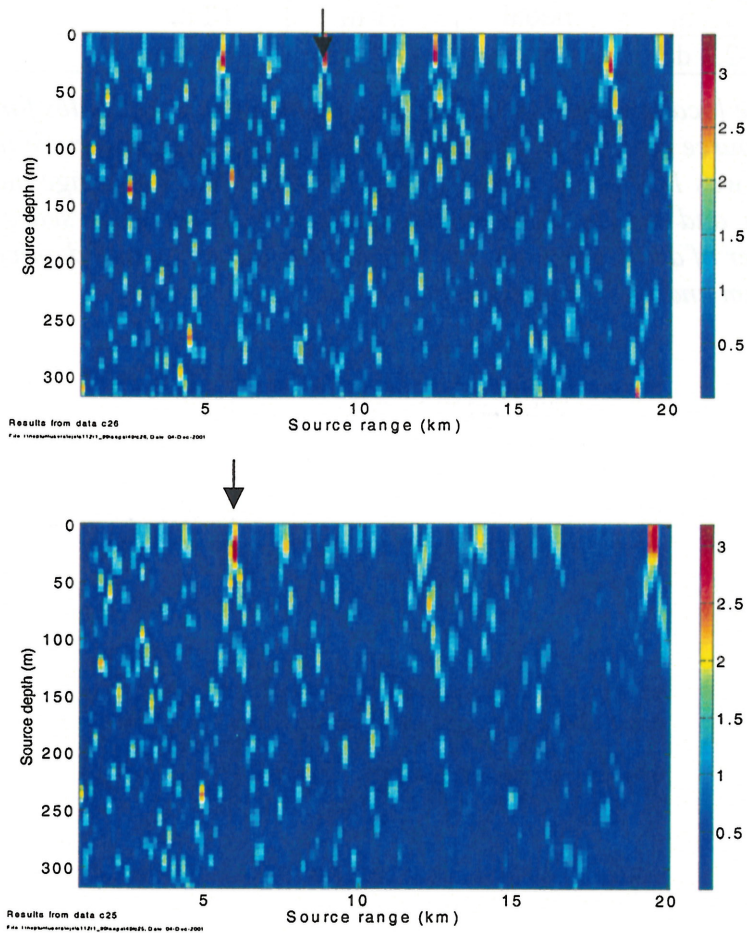

Figure 6.2   *Range-depth ambiguity surface at 48.9 Hz. Upper: baseline model. Lower: baseline model with GA estimated parameters at 48.9 Hz.*

Figure 6.3   Source localization at 40.4 Hz. The a posteriori distributions. Upper panel:
baseline modell. Range estimate GA best/ppd: 3.5 km, GA best/ppd: -2.76 dB,
GA mean: -36.7 dB. Lower panel: baseline model with GA estimated parameters
at 48.9 Hz. Range estimate GA best: 7.58 km, GA ppd: 2.8 km. Bartlett power
GA best: -4.05 dB, GA ppd: -4.20 dB, GA mean: -25.2 dB.

Results from data new02
File: I:\neptun\users\eje\s1121_89\esg.et4G\new02; Date: 05-Dec-2001

Figure 6.4   *Source localization at 48.2 Hz. The a posteriori distributions. Upper: baseline modell, GA ppd: -3.66 dB. Lower: baseline model with GA estimated parameters at 48.9 Hz, GA ppd: -3.44 dB .*

Figure 6.5   *Range-depth ambiguity surface at 48.2 Hz. Upper: baseline model. Lower: baseline model with GA estimated parameters at 48.9 Hz.*
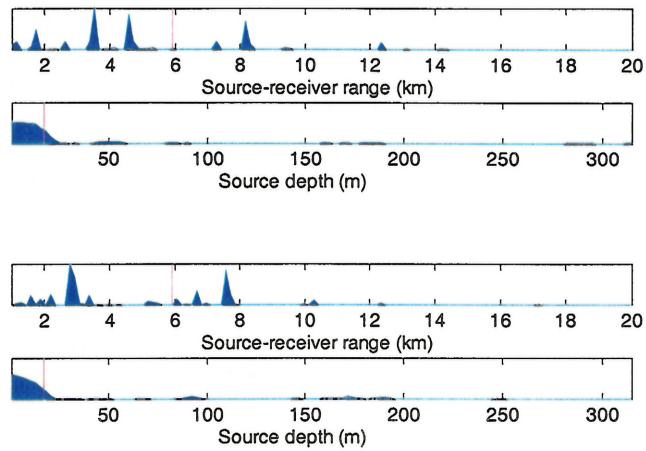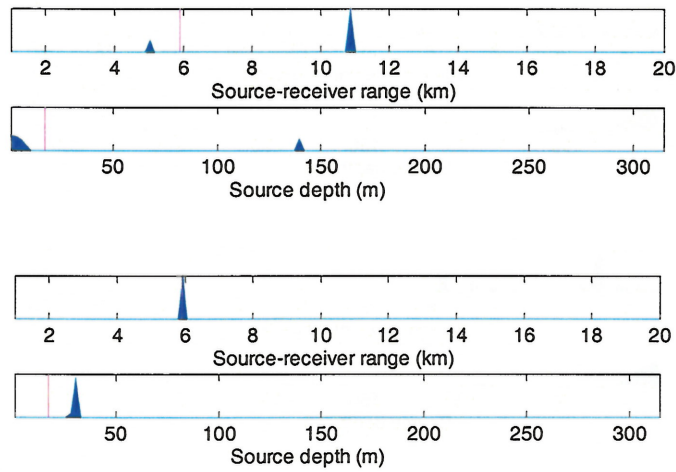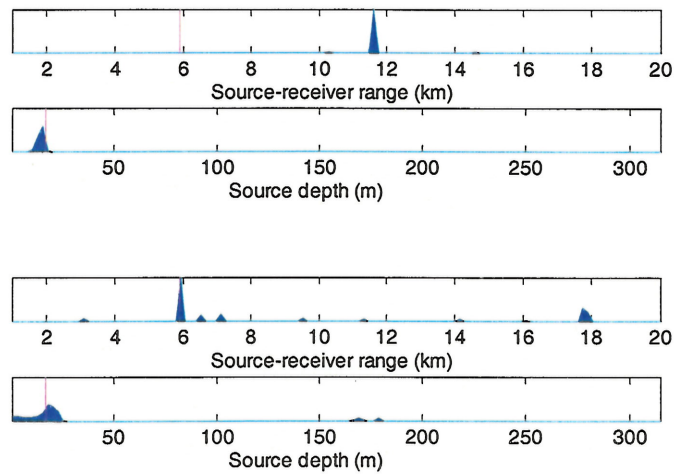
Figure 6.6   Source localization at 87.6 Hz showing the a posteriori distributions. Upper: baseline model, GA ppd: -4.28 dB. Lower: baseline model with GA estimated parameters at 48.9 Hz, GA ppd: -4.43 dB.
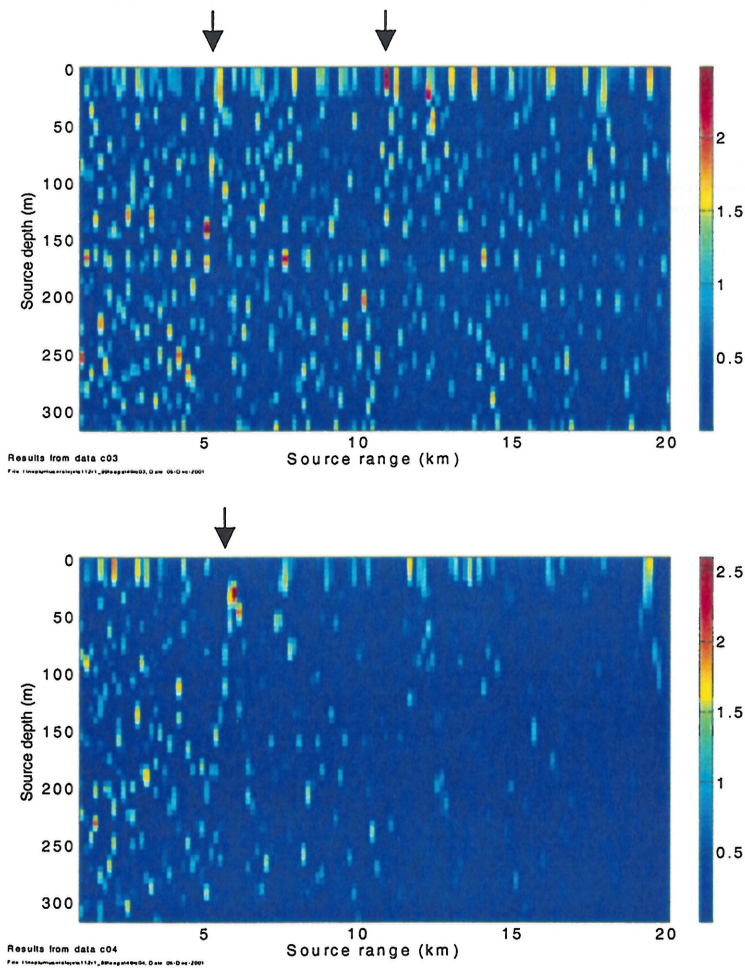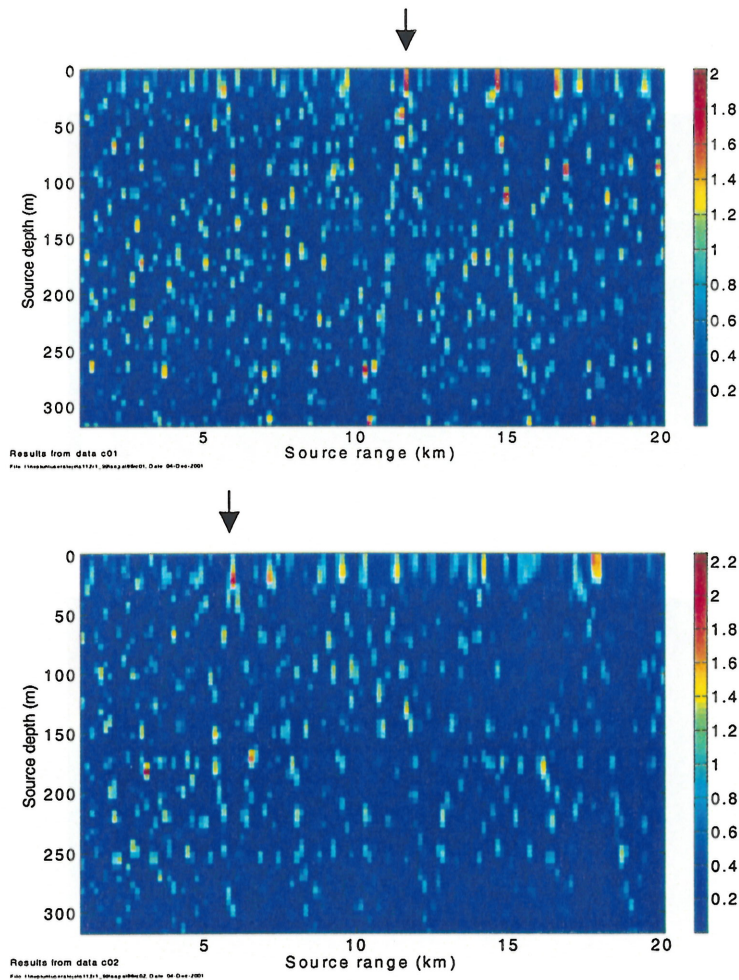

Figure 6.7   Range-depth ambiguity surface at 87.6 Hz. Upper: baseline model. Lower: baseline model with GA estimated parameters at 48.9 Hz.

Figure 6.8   *Source localization with covariance matrices at 40.4 Hz, 48.2 Hz and 87.6 Hz as input. The summation over frequency was incoherent. The a posteriori distributions are shown for two models. Upper: baseline model. Lower: baseline moel with GA estimated parameters at 48.9Hz.*

Figure 6.9   *Range-depth ambiguity surface when using the covariance matrices at 40.4 Hz, 48.2 Hz and 87.6 Hz as input. The summation over frequency was incoherent. Upper: baseline model. Lower: baseline model with GA estimated parameters at 48.9 Hz.*

7 SUMMARY AND RECOMMENDATIONS

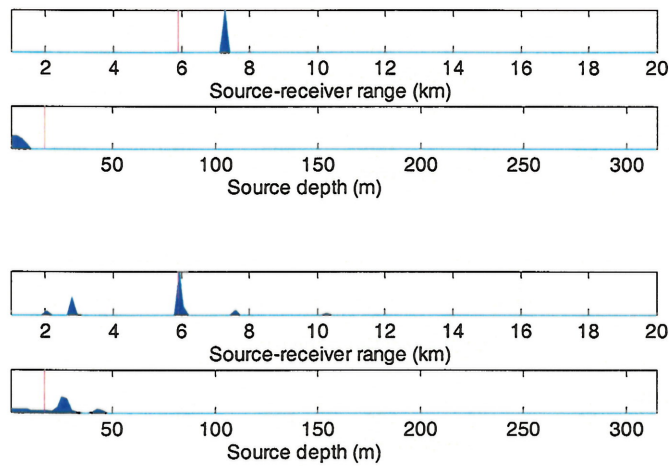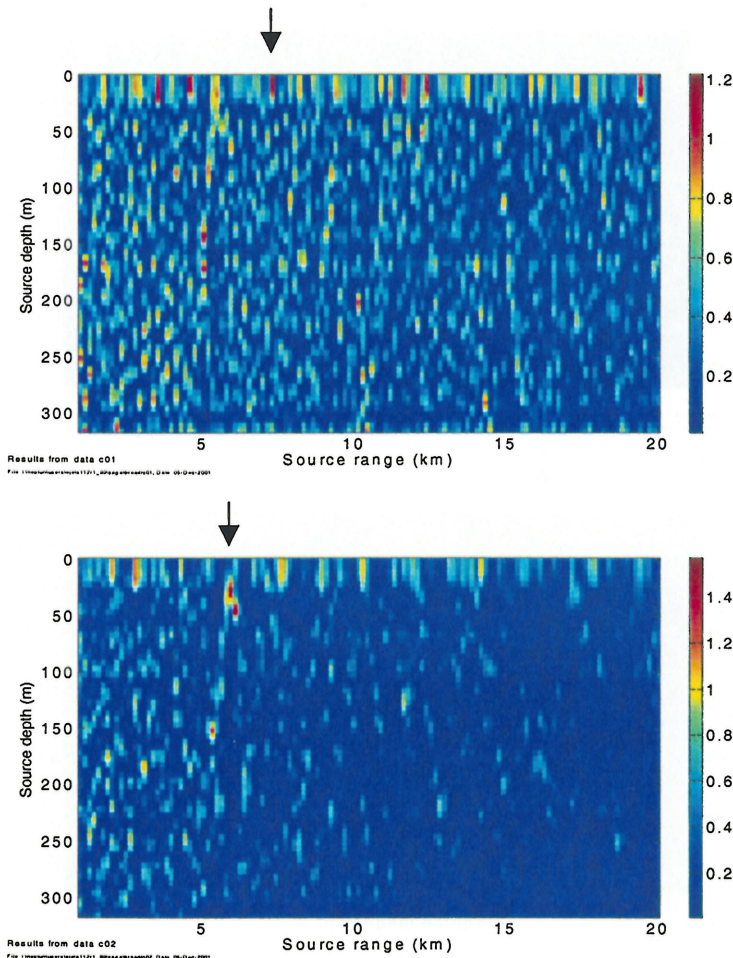Data from the L-antenna experiment in 1999 has been analysed and inverted with respect to geoacoustic/geometric parameters and source localization in this report, using the OASES modules OASP and OAST, and SAGA. No shear effects were addressed and the acoustic models were range-independent. Seismic measurements in the area showed weakly range-dependent bottom, with a sediment layer above the bedrock, with thickness ~37 m and average velocity ~1800 m/s. Refraction measurements showed an upper substrate velocity of about 2400 m/s.

The shot selected for analyses detonated at distance 5.91 km from the vertical antenna at a depth of 17.2 m. The signal received at the 21 hydrophones with spacing 10 m showed clear pulse arrivals. Simulation of the time responses indicated that the first and second bubble pulses in addition to the shock pulse dominated the signal. The direct and bottom-reflected pulses were unfortunately more or less absent due to the downward refracting sound velocity profile. This was confirmed by ray-tracing simulation.

The baseline model consisted of six layers: vacuum, three water layers, sediment layer and substrate layer (half-space). When optimising the water depth, sediment thickness, sediment velocity and substrate velocity at 48.9 Hz the GA best Bartlett power increased from −7.9 dB to 1.4 dB. The GA best parameter estimates for water depth, sediment thickness and sediment velocity were 328.1 m, 32.5 m, 1610 m/s and 2265 m/s respectively. The water depth was consistent with the average depth between receiver position and source position. Both the sediment velocity and sediment thickness was lower than expected. However, a sediment velocity down to 1600 m/s could indicate that only the upper sediment layer was influencing the acoustic propagation. Also different inversions and correlation plots showed that the substrate velocity was not very sensitive. Time response simulations over a wide frequency interval also indicated that the substrate velocity was not important for the propagation. Omitting the substrate layer in the baseline model however reduced the Bartlett power. When optimising the source depth and source-receiver range in addition to the water depth, sediment thickness, sediment velocity and substrate velocity, the GA best Bartlett power increased to −0.8 dB. However, the estimate for depth was not plausible.

Inversion at 22.9 Hz gave non-plausible parameter estimates, probably due to low signal-to-noise ratio. Inversion at 40.4 Hz and at 87.6 Hz gave parameter estimates in coherence with the parameter estimates found at 48.9 Hz. The Bartlett power decreased at these frequencies and the parameter estimates at 48.9 Hz were therefore incorporated in the baseline model in the source localizations. Inversion at 48.2 Hz gave multi-modal peaks in the *a posteriori* distributions.

Source localization was carried out at different frequencies for the baseline model and for the baseline model with GA estimated water depth, sediment thickness and sediment velocity at 48.9 Hz. The search space for the source-receiver range was 1 − 20 km, while the search space for the source depth was 1 − 315 m, covering about the whole water column. Generally, using the baseline model with GA estimated parameters at 48.9 Hz the source localization was very good, especially in range. The peak was located in the range cell closest to the true range (the

resolution in range was 150 m) in both single frequency localizations and in a multi-frequency localization. The source was also located in the upper layer of the water column. The exception was at 40.4 Hz, where the *a posteriori* distributions showed multi-modal peaks.

This report is the first on matched field processing of the L-antenna data from 1999. During the analyses several aspects of SAGA have been touched. In following up reports it is may be interesting to

- study the algorithms behind the *a posteriori* distributions
- study the genetic algorithms
- address other search methods than genetic algorithms

With regards to the presented results it would be interesting to

- reduce the search bands for range and depth in the source localizations and increase the resolution, in order to estimate the position more exact
- omitting half of the hydrophones in the input covariance matrix and use the other half for source localization
- open up the receiver depths and coupling the antenna to the bottom
- study the robustness of the GA parameter estimates
- analyse deeper shots and shots at other ranges
- address shear effects
- address range-dependence

APPENDIX

A ARRAY POSITION AND TILT

The planned array position, i.e. the centre of the array's horizontal part, was at 72°00.0' N and 030°00.0'E. The actual position was estimated based on several calibration shots and the closest shots from run 1 – 3. The vertical antenna was estimated to be 537 m ESE (inline) of the planned array position and 30 m NNE (offline). Based on the geometry onboard the source vessel and the GPS position of the vessel at drop/launch time it was possible to estimate the range between the detonation position and the vertical antenna for each shot.

The UTM and geographical coordinates of the array's vertical part are listed in Table A.1. The array bearing was estimated to be 295.7° in GRS80 system, and 293° in the UTM system (6).

	Geographical coordinates (GRS80)		UTM	
Planned array position	72°00.0'N	030°00.0'E	E 603433	N 7991509
Estimation of the actual position of the array's vertical part	71°59.8889'N	030°00.8676'E	E 603941	N 7991327

Table A.1   Relevant coordinates of the hydrophone array.

The tilt of the vertical antenna was monitored continuously during the experiment using three Aquadopp current meters. The current meters were fastened to the array cable with strips and tapes approximately 194 m, 104 m and 14 m above the lowest hydrophone, which after the deployment was 4 m above the sea floor. The tilt direction for the upper two current meters, when tilted, was east-southeast, while the lower current meter tilted in the east-west plane. The tilts of the lowest, middle and upper current meter were at most 14°, 10° and 6°, respectively.

Figure A.1 shows the magnitude of the sensor tilts during the last part of run 1 (which started at 4/8–99 at 16:30 and terminated 5/8-99 at 02:43), when the source vessel was heading WNW towards the antenna. By the time run 1 ended, the tilts of the upper and middle current meter were at minimum (approximately 0.2°), indicating that the vertical antenna cable was quite linear. However, the lower current meter, which was 18 m above the sea floor, experienced at tilt of 4 - 5°.

Two possible situations of the cable curvature are modelled in Figure A.2. In the first case the cable has a break point midways between the two lower sensors, and the upper two sensors will then have a displacement of 4 – 5 m. The bottom sensor is estimated having a displacement of less than 1.5 m. In the second case the break point is at the bottom sensor, and all three sensors will the experience a displacement of less than 1.5 m. The changes in sensor depths are negligible in both cases. With an acoustic source signal of 50 – 100 Hz these displacements are well below the wavelength of the signal (30 – 15 m).
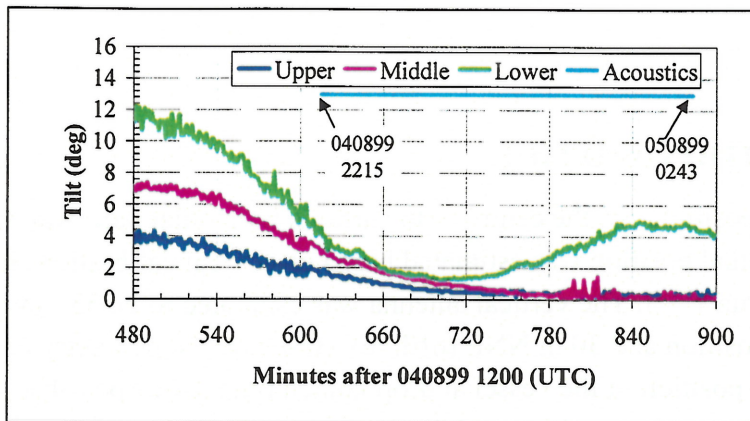
Figure A.1 Three Aquadopp current metes were mounted on the vertical array at depths 121 m, 211 m and 301 m. The figure shows the magnitude of the tilts during the last part of run 1 (marked as a light blue line), when the source vessel was heading WNW towards the antenna).
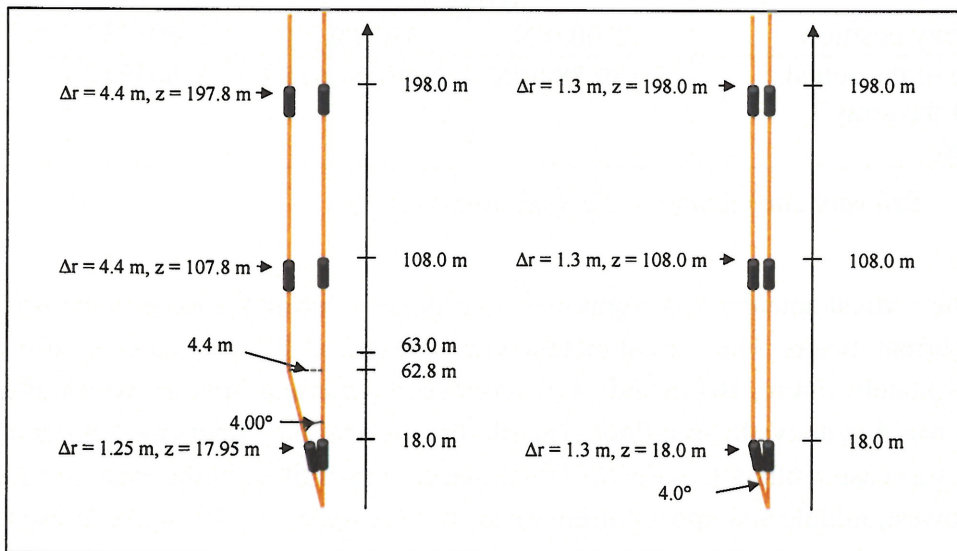
Figure A.2 Illustrations of the curve of the vertical array cable by the end of run 1. The current meters measured approximately 4°, 0° and 0° tilts from bottom to top. The instruments were fastened to the cable 18 m, 108 m and 198 m above the sea floor. Left: the cable is modelled having one break point midways between the bottom and middle sensor. Right: the cable is modelled having one break point at the bottom sensor. In both cases the horizontal displacement of the bottom sensor is less than 1.5 m. In the worst case the horizontal displacement is 4 – 5 m.

B OCEANOGRAPHY

During the experiment five CTD measurements were taken at the receiver position and the sound speed profiles are plotted in Figure B.1. In general there was a warmer surface layer of thickness 20 – 40 m, with sound velocity 1481 – 1488 m/s, and a colder bottom layer with sound velocity down to 1463 m/s. The average sound velocity during the experiment was 1472 m/s at the receiver position.

At the source position five XCTD's, five XSV's and several XBT's were dropped. The sound speed profiles computed from the XCTD's are plotted in Appendix B. In general, the tendency is the same at both the source position and receiver position.
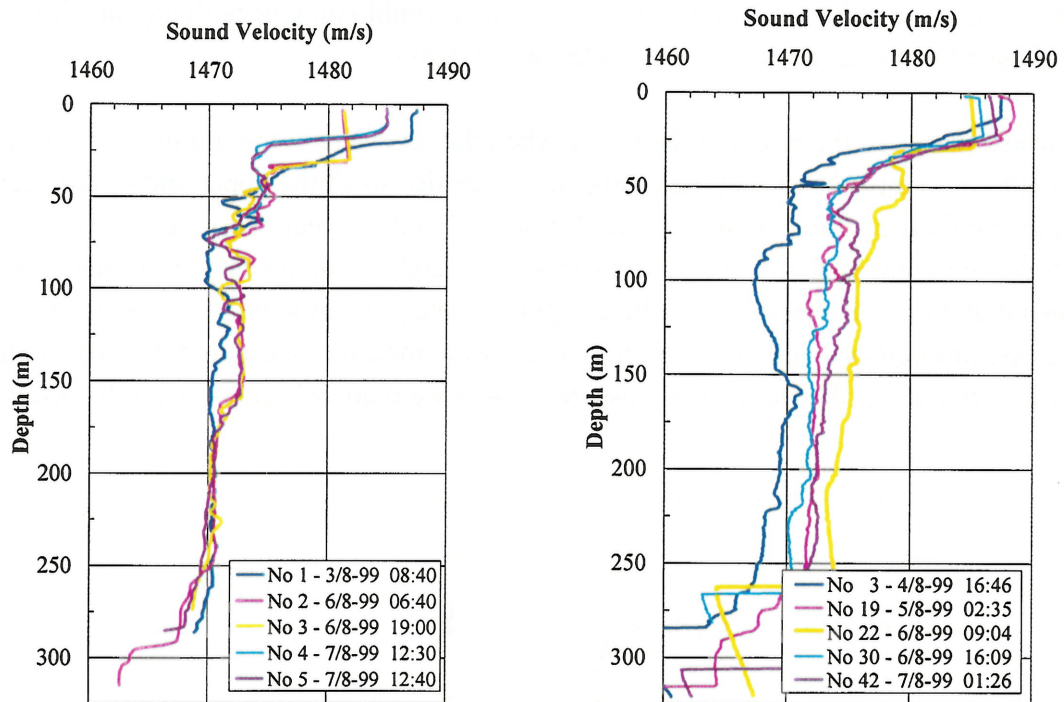

Figure B.1   The sound velocity profiles at the receiver position (left) and source position (right). The numbering is individual at each position.

C BATHYMETRY

The average water depth at the antenna position was measured indirectly from pressure sensors within the upper two Aquadopp current meters. The two pressure sensors recorded their depths continuously during the experiment, while a pressure sensor within the third current meter was too deep to logging data.

During the period from 4/8 at 04:00 to 7/8 at 07:00 the average depths of the two upper current meters were 121.5 m and 211.5 m. The recorded sensor depths varied from -1 m to + 3 m during the experiment, in phase with the sensor tilts (which varied in phase with the current velocity). Hence the variations in sensor depths were a combination of both the physical tilting of the instruments and an actual increase in the water depth.

A simple estimation of the effect of the tilting when the tilts were at maximum (14°, 10° and 6° from bottom to top) shows that the change in sensor depths of the upper and middle current meter due to only the tilting could easily be 3.6 m and 2.9 m respectively, see Figure C.1. The tilting could therefore explain the variations in sensor depths. The lowest current meter would have been only minor affected by the tilting (approximately 0.5 m with a tilt of 6°), and a well working pressure sensor within this current meter would therefore measured directly the tide changes in water depth. However, the pressure sensors were not specified to depths below 200 m.
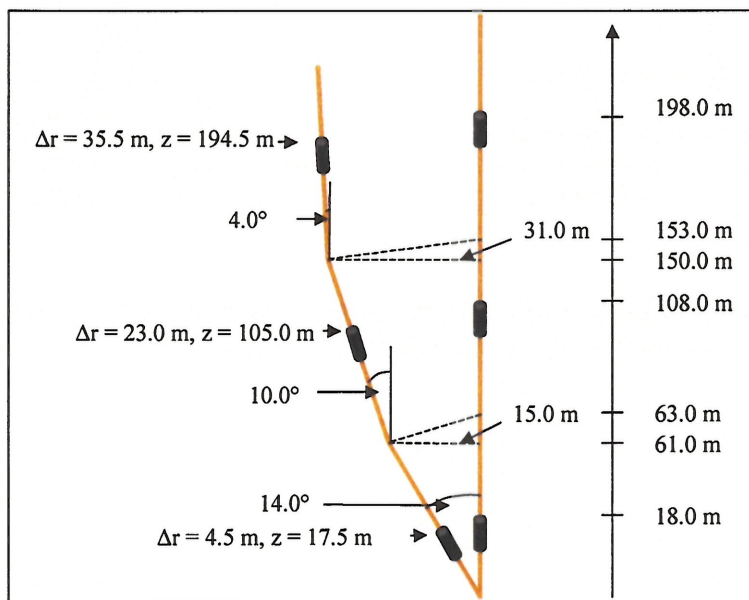

Figure C.1   *Illustration of the change in sensor depths when the sensor tilts are at maximum. The three Aquadopp current meters were fastened to the array cable 18 m, 108 m and 198 m above the sea floor (anchor). The tilted cable is modelled as three straight lines, where the two break points are midway between the closest current meters.*

When the current velocity was at minimum there was presumably either low tide or high tide. Looking at the depth data at moments with minimum current velocity, depth variations of less than 1 m are observed between adjacent velocity minima (one low tide and one high tide). This suggests that the tidal influence on the water depth was less than 1 m. During minimum current velocity, the sensor depths are approximately 0.5 – 1.0 m less than the stated average sensor depths, see Figure C.2. Taking into account the distances along the cable from the sea floor to the two upper current meters (108 m and 198 m), this suggests that the water depth in the area was approximately 319 m ± 0.5 m.

During the deployment of the array the water depth at the antenna position was measured directly using an EA 500 echo sounder from Simrad (38 kHz). The deployment was carried out in the afternoon 3/8 and the depth where the array's vertical part was located, was logged to be 329 m, assuming a sound velocity 1500 m/s. Subtracting 4 m due to depth calibration errors in the instrument and taking into account the actual sound velocity in the water column (1472 m/s in average), the echo sounder measured a water depth of 319 m, confirming the result from the Aquadopp current meter measurements.

Assuming a water depth of 319 m, the depth of the lowest hydrophone was 315 m, while the depth of the upper hydrophone was 115 m at minimum tilt (and minimum current velocity).
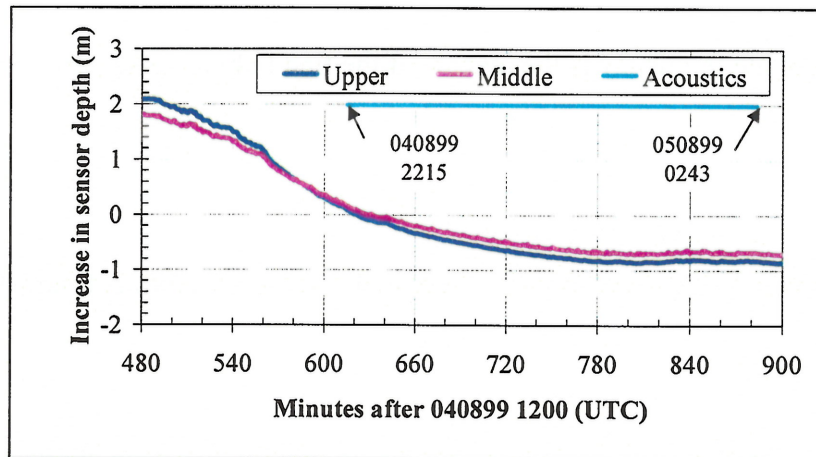

Figure C.2   *The change in sensor depths for the upper and middle current meter during the last part of run 1 (marked with light blue line), when the source vessel was heading towards the antenna). At the end of the run, the sensor depths were 0.5 – 1.0 m less than the stated average depths of 121.5 m and 211.5 m.*

D BUBBLE PULSE PERIODS AND PRESSURES

Based on the first bubble pulse period it is possible to estimate the actual detonation depth of the SUS charges, assuming constant charge weight. The bubble pulse period is given as (9)

$$T_i = K_i w^{1/3} / (z + 10.1)^{5/6} \qquad\qquad (D.1)$$

where T_i is the bubble pulse period of the ith bubble pulse in seconds, w is the charge weight in kg and K_i is a constant for the ith bubble pulse given as

$$K_1 = 2.11$$
$$K_2 = 1.48 \qquad\qquad (D.2)$$
$$K_3 = 1.20$$

T_2 is defined as the delay between the first and second bubble pulse (in seconds), T_3 is the period between the second and third pulse etc. The detonation depth z in meters is related to the hydrostatic depth z_0 in meters

$$z = z_0 - 10.1 \qquad\qquad (D.3)$$

The fundamental bubble frequency is the inverse of the first bubble pulse period

$$f_1 = \frac{1}{T_1} \qquad\qquad (D.4)$$

When measuring the bubble pulse period T_1 the actual detonation depth is found as

$$z = (K_1 w^{1/3} / T_1)^{6/5} - 10.1 \qquad\qquad (D.5)$$

There is a vertical migration of the bubble pulses due to gravity. For deep charges it is possible to ignore this effect. The critical *detonation* depth is approximately (9) (10)

$$z_c = 75 \, w^{1/4} - 10 \qquad\qquad (D.6)$$

which for SUS charges with 0.82 kg TNT is approximately 60 m. A 18 m shot will therefore experience migration and the bubble pulse periods will increase as the bubble rises during the oscillations.

Semi-empirical relationships for the peak pressures of the shock pulse and of the first and second bubble pulses are found in (9),

$$P_0 = 5.04 \cdot 10^{13} \left(w^{1/3} / R \right)^{1.13}$$

$$P_1 = 1.49 \cdot 10^{12} \left(w^{1/3} / R \right) z_0^{0.33} \tag{D.7}$$

$$P_2 = 3.93 \cdot 10^{11} \left(w^{1/3} / R \right) z_0^{0.28}$$

where z_0 is the hydrostatic depth in meters and R is the range in meters.

As seen the pressure of the first and second bubble pulses are dependent on the depth. This depth dependence is an improvement in earlier empirical results, taking into account the migration effect of the bubble pulses, which is as mentioned more dominant for shallow charges than for deep charges (9). The pulse pressures are in fact more sensitive to migration than the pulse periods.

E   THE NUMBER OF MODES

The number of modes M of a Pekeris waveguide (assuming iso-velocity water layer and a half-space bottom) is given as (15)

$$M \leq \frac{2Df}{c_0} \sqrt{1 - \left(\frac{c_0}{c_1}\right)^2} \tag{E.1}$$

where f is the frequency of the signal, D is the water depth and c_0 and c_1 are the sound velocities in the water and bottom, respectively. The number of modes for different frequencies and water depths is listed in Table E.1. As seen a depth change from 319 m to 326 m is not introducing more modes at 50 Hz, nor at 90 Hz. However decreasing the sound velocity in the bottom from 1800 m/s to 1645 m/s reduces the number of modes from 12 to 9 at 50 Hz and from 22 to 17 modes at 90 Hz.

Water depth (m)	319	319	319	319	326	326
Frequency (Hz)	22	50	90	50	50	90
Sound velocity in water (m/s)	1473	1473	1473	1473	1473	1473
Sound velocity in bottom (m/s)	1800	1800	1800	1645	1645	1645
Maximum number of modes	5	12	22	9	9	17

Table E.1   Estimations of the number of normal modes for different frequencies, water depths and bottom sound velocities.

F OASP

The OASES module OASP was used for simulating the time series. The maximum FFT range is equal to (4)

$$R_{MAX} = \frac{NW}{FREQ\left(\frac{1}{CMIN} - \frac{1}{CMAX}\right)} = \frac{NW}{\left(k_{MAX} - k_{MIN}\right)} 2\pi \tag{F.1}$$

where FREQ is the centre frequency of the source pulse (also called FRC or f_c) , k_{max} and k_{min} are the maximum and minimum wavenumbers, respectively, cmax and cmin are the maximum and minimum phase velocity, respectively and NW is the number of wavenumber samples

Automatic wave number sampling was selected (NW = - 1), in order to have fully flexibility. However this require more computational time. If not automatic wave number sampling is selected, the number of wavenumber samples must satisfy

$$NW \geq R_{MAX} \frac{FREQ}{CMIN} \tag{F.2}$$

The low frequency limit in the frequency integration, F1, is free to decide, but the upper frequency limit F2 is limited by the time sampling increment according to (4)

$$F2 \leq \frac{0.5}{DT} = f_{Nyquist} \tag{F.3}$$

Thus, if F2 is set higher than the value accepted by the time sampling increment, OASES reduces F2 automatically. In order to increase F2, the time sampling increment must be reduced. OASES recommends to use a time increment equal to 0.1 divided by the centre frequency for the source pulse, and in this case $F2 \leq 5\,FREQ$.

An example of the OASP input file is shown in Figure F.1.

```
INFORMATION LINE
N 1 J 1        !OASP options
120.0  0.0     !Source frequency, integration contour offset
6              !# layers
0        0.0000  0      0.00   0      0.00   0
0        1488.0  0      0.00   0      1.00   0
30       1473.0  0      0.00   0      1.00   0
275      1465.0  0      0.00   0      1.00   0
319      1800.0  0      0.50   0      2.00   0
356      2400.0  0      0.10   0      2.20   0
17.2           !Source depth (mean)
115 315 21     !Min and max receiver depths, # receivers
1000 1E8       !Min and max phase velocity
-1 0 0 0       !Automatic wavenumber sampling
16384  4.0 700.0 0.0008 5.91 5.91  1   !# time samples, min and max frequency,
               time sampling increment (s), first range (km), range increment (km), # ranges
```

Figure F.1   Example of OASP data file for generating time responses on a vertical array.

G SAGA AND OAST

The inversion of acoustic field observations may be separated into geoacoustic and geometric inversion, and source localization. In geoacoustic and geometric inversion the goal is to estimate the geoacoustic and/or geometric parameters (sound speeds, water depth, sediment thickness, shear velocities etc). In localization the geoacoustic and geometric parameters are assumed known, and the acoustic field is inverted with respect to source depth and source range.

In both cases the inversion may be separated into five parts (5)

1) Discretization of the environment and discretization or transformation of the input data
2) Efficient and accurate forward modelling
3) A suitable objective function
4) Efficient optimisation procedures
5) Uncertainty analysis

First, the seismo-acoustic environment is discretized into M environmental parameters contained in a model vector $m^T = [m^1, m^2, .., m^M]$. The search space for the parameter i is discretized into 2^{n_i} values (user selected) according to

$$\Delta m_i = \frac{m_i^{max} - m_i^{min}}{2^{n_i} - 1}$$ (G.1)

where m_i^{max} and m_i^{min} are the upper and lower bound of the search space for parameter i (user selected).

The optimisation is carried out to find the optimum model parameter vector m that minimizes the selected objective function, which contain both the measured field and the replica field from the forward modelling. The field may be given as the complex pressure, covariance matrix, transmission loss etc). When there is a perfect match, the energy of objective function is zero.

The covariance matrix was input data in the inversions in this report. The matrix was computed using the interactive data language IDL for Windows according to

$$R(k) = p(k) \, p^*(k)$$ (G.2)

where p(k) is the measured complex pressure (or more often the complex voltage), $p^*(k) = \overline{p(k)}^T$, $p(k)^T = [p_1(k) \quad ... \quad p_N(k)]$, k is the frequency bin and the frequency is given relative to the sample frequency f_s as $f = \frac{k}{N} f_s$.

The complex pressure at hydrophone j is defined as the fast Fourier transform of the measured time series at hydrophone j as

$$p_j(k) = \frac{1}{N} \sum_{n=1}^{N-1} x_j(n) e^{-i2\pi kn/N}$$

(G.3)

where N is the number of time samples or the FFT length.

The covariance matrix is normalised by dividing with the norm of the pressure vector squared, that is (13),(14), (16).

$$C(k) = \frac{p(k)\, p^*(k)}{\|p(k)\|^2} = \frac{R(k)}{\|p(k)\|^2}$$

(G.4)

The objective function used in the inversions is the Bartlett processor. In literature the processor is defined in different ways (12), (13), (14),(16). The no-normalised processor may be defined as (when perfect match gives zero energy)

$$
\begin{aligned}
\Phi &= \sum_{j=1}^{N_{dep}} \left[R_{jj} - q_j^* \sum_{l=1}^{N_{dep}} R_{jl} q_l \right] \\
&= p^* p - \sum_{j=1}^{N_{dep}} q_j^* p_j \sum_{l=1}^{N_{dep}} p_l^* q_l \\
&= \|p\|^2 - \left| \sum_{j=1}^{N_{dep}} q_j^* p_j \right|^2 \\
&= \|p\|^2 - q^* p p^* q \\
&= \|p\|^2 - q^* R^* q
\end{aligned}
$$

(G.5)

where R is the covariance matrix (not normalized), p is the measured complex pressure vector (not normalized) and q is the forward model prediction vector (normalized).

Note that the output of the Bartlett processor, Φ, is dependent on the magnitude of the input data. Hence, special care should be taken when comparing the output of the Bartlett processor (energy) from different input data.

The normalized Bartlett processor is equal to

$$\Phi^N = 1 - \frac{q^* R q}{\|p\|^2} = 1 - \frac{q^* p p^* q}{\|p\|^2} = 1 - \frac{\left(q^* p\right)\left(q^* p\right)^*}{\|p\|^2} = 1 - q^* C q$$

(G.6)

where $C = \dfrac{R}{\|p\|^2}$ is a normalized covariance matrix.

A covariance matrix may be normalized in SAGA using option b (normalized by the norm squared as above or option B (normalized by the largest eigenvalue of the covariance matrix). In the inversions, the covariance matrix was normalized in IDL by the norm squared.

During the optimisation, all obtained samples of the search space are stored and used to estimate the *a posteriori* probabilities. For simplicity the marginal probability distributions are plotted. Based on the *a posteriori* probability distributions, three estimates for the model parameters are available in the *.out file from SAGA: those associated with the largest fit or lowest energy (best fit), those based on the peak of the distribution (PPD) and those based on the mean of the distributions (mean)(12),(13). In addition, the standard deviation of the distribution expressed as a fraction of the search interval of each parameter is given (12). The energy of the Bartlett processor is given for all three cases.

The *.plt file from the post processing contains the output from SAGA. If option p is selected, the measured and calculated pressures across the array are plotted for comparison. The pressures plotted are normalized according to

$$p_j^{plot} = \frac{|p_j|}{\sum_{j=1}^{N_{dcp}} |p_j|} \quad \text{and} \quad q_j^{plot} = \frac{|q_j|}{\sum_{j=1}^{N_{dcp}} |q_j|} \tag{G.7}$$

The Bartlett power is plotted when option p3 is selected. The Bartlett power versus depth of the measured data is defined as the magnitude squared of the pressure vector, divided by the norm of the pressure vector squared, that is (13)

$$BP_j^{OBS} = \frac{|p_j|^2}{\|p\|^2} \tag{G.8}$$

When the covariance matrix is input data, the pressure vector is estimated as the first eigenvector of the covariance matrix. The magnitude of the eigenvector equals the magnitude of the pressure vector if no noise.

The Bartlett power versus depth of the calculated data (replica field) is equal to

$$BP_j^{CAL} = \frac{Re(\overline{q_j p_j})\overline{(q^* p)}}{\|p\|^2} \tag{G.9}$$

where q is the calculated (normalized) pressure vector based on the model vector giving the lowest energy (best fit between measured data and calculated data).

The Bartlett power in dB as given in the *.out file is by experience found to be

$$BP^N(dB) = 10\log\left(1 - \Phi_{mean}^N\right) \tag{G.10}$$

If the covariance matrix is not normalised the Bartlett power is equal to

$$BP(dB) = 10 \log \left(\|p\|^2 - \Phi_{mean} \right) \tag{G.11}$$

The relationship between these two expressions of the Bartlett power is

$$BP^N(dB) = BP(dB) - 10 \log \left(\|p\|^2 \right) \tag{G.12}$$

If the complex pressure vector is input data, the Bartlett power in dB as given in the *.out file is by experience found to be

$$BP^N(dB) = 10 \log \left(\Phi^N_{mean} \right) = 10 \log \left(\frac{\Phi_{mean}}{\|p\|^2} \right) \tag{G.13}$$

It is surprisingly that the Bartlett power is defined in this way. The better match, the larger power in magnitude

In order to have relative energies it is necessary to normalise the pressure vector according to

$$p_j = \frac{p_j}{\|p\|} \tag{G.14}$$

If more than one frequency is selected, the Bartlett processor is equal to

$$\Phi = \sum_{i=1}^{N_{freq}} \sum_{j=1}^{N_{dep}} \left[R_{jj,i} - q^*_{ij} \sum_{l=1}^{N_{dep}} R_{jl,i} q_{il} \right] \tag{G.15}$$

The summation over frequency is incoherent.

Figure G.1 shows an example of the input data file.

INFORMATION LINE							
W c r A p3 b			!SAGA options				
5000 64 64			!# forward runs, population size , # populations				
0.8 0.5 0.05							
N I J T			!OAST options				
48.9 48.9 1			!Frequency				
6			!# layers				
0	0.0	0	0.00	0	0.00	0	
0	1488.0	0	0.00	0	1.00	0	
30	1473.0	0	0.00	0	1.00	0	
275	1465.0	0	0.00	0	1.00	0	
319	1800.0	0	0.50	0	2.00	0	
356	2400.0	0	0.10	0	2.20	0	
17.2			!Source depth (mean)				
115 315 21			!Min and max receiver depths, # receivers				
1000 1E8			!Min and max phase velocities (m/s)				
-1 1 1			!Automatic wavenumber sampling				
1			!#ranges				
5910			!Range (m)				
7				!#inversion parameters			
2	2	1450	1495	32	!Water velocity, upper layer		
2	3	1450	1495	32	!Water velocity, middle layer		
2	4	1450	1495	32	!Water velocity, lower layer		
2	5	1490	2000	128	!Sediment velocity		
2	6	1490	3500	128	!Substrate velocity		
1	5	315	335	32	!Water depth		
7	5	1	51	64	!Sediment thickness		

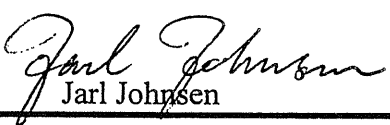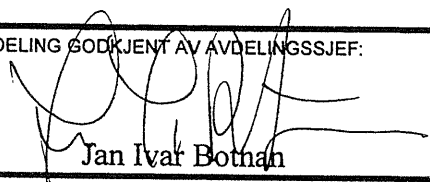*Figure G.1   Example of SAGA data file for geoacoustic inversion.*

References

(1) Eidem E J, Bendiksen B, Helgesen H (1999): Project Swasi: Technical Cruise Report from Phase S-V 1999, FFI/RAPPORT-99/04955, Exempt from public disclosure

(2) Johnsen J (1999): SWASI II - Cruise Report, Phase S-V 1999, FFI/NOTAT-99/05715, Exempt from public disclosure

(3) Solberg C E (2001): Geoakustiske modeller for MFP eksperiment i Barentshavet august 1999, FFI/RAPPORT-2001/00335

(4) Schmidt H (1999): OASES Version 2.1: User Guide and Reference Manual, Massachusetts Institute of Technology, USA.

(5) Gerstoft P (1999): SAGA User Manual 3.0: An inversion software package, SACLANTCEN and Marine Physical Laboratory

(6) Eidem E J (2000): Estimation of the Hydrophone Array Position During Swasi 1999 Phase S-V, FFI/RAPPORT-2000/04107, Exempt from public disclosure

(7) Eidem E J (2000): A 1040 m Deployable Hydrophone Array and its Data Acquisition System - Part II: Detailed description, FFI/RAPPORT-2000/04034, Exempt from public disclosure

(8) Eidem E J (2000): A 1040 m Deployable Hydrophone Array and its Data Acquisition System - Part II: General description and data formats, FFI/RAPPORT-2000/04034, Exempt from public disclosure

(9) Chapman N Ross (1985): Measurement of the waveform parameters of shallow explosive charges, *JASA* **78**, 2, 672-681.

(10) Weston D E (1960): Underwater Explosions as Acoustic Sources, *Proc Phys Soc* **76**, 2, 233-249.

(11) Chapman N R, Lindsay C E (1996): Matched-Field Inversion for Geoacoustic Model Parameters in Shallow water, *IEEE Journal of Oceanic Engineering* **21**, 4, 347-354.

(12) Gingras D F, Gerstoft P (1995): Inversion for geometric and geoacoustic parameters in shallow water: Experimental results, *JASA* **97**, 6, 3589-3598.

(13) Gerstoft P, Gingras D F (1996): Parameter estimation using multifrequency range-dependent acoustic data in shallow ater, *JASA* **99**, 5, 2839-2850.

(14) Gerstoft, P (1994): Inversion of seismoacoustic data using genetic algorithms and *a posteriori* probability distributions, *JASA* **95**, 2, 770-782.

(15) Jensen F B et al (2000): Computational Ocean Acoustics, Springer, New York, USA, 578.

(16) Gerstoft P, Mecklenbräuker C F (1998): Ocean acoustic inversion with estimation of a posteriori probability distriutions, *JASA* **104**, 2, 808-819.

DISTRIBUTION LIST

FFIBM   **Dato:** 5 november 2001

RAPPORTTYPE (KRYSS AV)			RAPPORT NR.	REFERANSE	RAPPORTENS DATO
X RAPP	☐ NOTAT	☐ RR	2001/02927	FFIBM/786/115	5 november 2001

RAPPORTENS BESKYTTELSESGRAD	ANTALL EKS UTSTEDT	ANTALL SIDER
Unclassified	32	63

RAPPORTENS TITTEL	FORFATTER(E)
SINGLE SHOT INVERSION FROM THE L-ANTENNA EXPERIMENT IN 1999	EIDEM Ellen Johanne

FORDELING GODKJENT AV FORSKNINGSSJEF:	FORDELING GODKJENT AV AVDELINGSSJEF:
Jarl Johnsen	Jan Ivar Bothan

EKSTERN FORDELING

ANTALL	EKS NR	TIL
		FO/E
1		Ved: Asgeir Berg
		US Naval Oceanographic Office
1		Att: Richard Simmons
		Stennis Space Center
		MS 39522-5002, USA

INTERN FORDELING

ANTALL	EKS NR	TIL
14		FFI-Bibl
1		Adm direktør/stabssjef
1		FFIE
1		FFISYS
1		FFIBM
4		FFIBM/Horten
1		Ellen J Eidem, FFIBM/Horten
1		Trond Jenserud, FFIBM/Horten
1		Connie E Solberg, FFIBM/Horten
1		Torgeir Svolsbru, FFIBM/Horten
1		Knut A Søstrand, FFIBM/Horten
1		Dag Tollefsen, FFIBM/Horten
1		Jens Hovem, FFIBM/Horten
1		Jarl Johnsen, FFIBM/Horten

FFI-K1   Retningslinjer for fordeling og forsendelse er gitt i Oraklet, Bind I, Bestemmelser om publikasjoner for Forsvarets forskningsinstitutt, pkt 2 og 5. Benytt ny side om nødvendig.